공학박사 학위논문

Development of Hydrogen Cold Cathode Penning Ion Source in Pulsed Operation with High Monatomic Fraction

높은 단원자 분율을 가진 펄스 운전 수소 냉음극 페닝 이온원 개발

2019 년 2 월

서울대학교 대학원

에너지시스템공학부(원자핵공학)

최 규 민

Development of Hydrogen Cold Cathode Penning Ion Source in Pulsed Operation with High Monatomic Fraction

지도교수 황 용 석

이 논문을 공학박사 학위논문으로 제출함

2018 년 10 월

서울대학교 대학원

에너지시스템공학부(원자핵공학)

최 규 민

최규민의 박사 학위논문을 인준함

2018 년 12 월

위 원 장 김 곤 호 (인)

부위원장 황 용 석 (인)

위 원 정 경 재 (인)

위 원 홍 인 석 (인)

위 원 김 한 성 (인)

Abstract

Development of Hydrogen Cold Cathode Penning Ion Source in Pulsed Operation with High Monatomic Fraction

Kyumin Choe

Department of Energy System Engineering

(Nuclear Engineering)

The Graduate School

Seoul National University

The hydrogen (proton or deuteron) ion source is an important part of the injector of the accelerator, the neutral beam injector of nuclear fusion, and the neutron generator. One of the most important performance factors of the ion sources is the ion beam current. The larger the beam current, the higher the yield of the target reaction. In the

case of the hydrogen ion sources, the monatomic fraction is also an important performance factor. The hydrogen ion beam also contains molecular ions (H_2^+ (D_2^+) or H_3^+ (D_3^+)) as well as monatomic ions (protons, H^+ or deuterons, D^+). The monatomic ions in the ion beam have a larger energy per a nucleon than the molecular ions, so the ion beam can improve the yield of the target reaction. Thus, the higher the monatomic fraction, the better the ion source performance. Among the type of hydrogen ion sources, Penning ion source, which is simple in structure and easy to configure power source, is mainly used for a portable sealed tube neutron generator. Penning plasma discharge has high plasma density even at low pressure due to confining more electrons in the discharge volume, which consists of the anode, the cathodes and the axial magnetic field. However, in the case of the portable sealed tubes, the limit of the structure makes the monatomic fraction only about 10%. Therefore, improving the monatomic fraction can improve the performance of the device which uses the ion beam from the ion source. In this study, I try to improve the performance of Penning ion source by enhancing the limit of the monatomic fraction.

As the equations, such as the particle balance equations describing the generation and the destruction of each ion species, atoms, and molecules, are calculated in parallel, based on the collision reactions of electrons, hydrogen molecules, atoms, and ions in the hydrogen plasma, the ion species fraction can be predicted according to the plasma parameters. From this numerical model, it can be seen that the higher the monatomic fraction of the hydrogen ion beam is acquired at the higher the plasma density, the lower electron temperature, and the lower the operating pressure. Adjusting the parameters of plasmas can improve the monatomic fraction of the ion beam.

The plasma density plays a major role among the plasma parameters affecting the monatomic fraction. The plasma density increases easily when a large amount of power is applied. However, it requires more cost, and damages the device quickly. Particularly, in the case of a portable device, there is a limitation in the structure and the power supply, so the power cannot be supplied infinitely. A hollow cathode structure, which can be used together with a DC power supply system of Penning ion source and which is simple in structure change, is proposed to modify Penning ion source. The plasma density enhancement due to the hollow cathode effect combining with Penning discharge makes the monatomic fraction higher. In addition, there is also an advantage that the lifetime of the device can be increased due to the resistance to the cathode degradation of the hollow cathode.

A time-of-flight mass analyzer is constructed and measured for the ion species fraction of the hydrogen ion beam. The mass analyzer utilizing magnetic field is generally used to measure the mass-to-charge ratio of the ion beam, but it is not appropriate to measure the ion species fraction of ion beam generated in a short pulse because the scanning speed of the magnetic field is slow. Therefore, I developed a time-of-flight mass analyzer capable of measuring the ion species fraction with only a short beam pulse packet. In particular, this study improved the signal-to-noise ratio of the measured signal by 50% through improving the gating device, which is a key component in cutting the ion beam into a short pulse packet.

The Penning ion source with hollow cathodes is operated with a magnetic field of 700 G after the optimization. When operating at a discharge current, about 2 A, considering the prevention of the damage of the cathodes, it was possible to obtain a monatomic fraction close to 60%, which is 5 – 6 times better than that of the

conventional device, which is about 10%. Moreover, the beam current density was more than twice as high as that of the general plane cathodes Penning ion source.

The result of this study will contribute to the future development of applications of Penning ion sources, and it is expected to show improved performance especially in the field of portable sealed tube neutron generator.

Keywords: Penning ion source, Hydrogen ion beam, Neutron generator, Monatomic fraction, Hollow cathode, Time-of-flight mass spectrometry

Student number: 2013-30300

Contents

List of Figures

List of Tables

Chapter 1 Introduction

1.1 Hydrogen Ion Sources and Their Applications

Hydrogen ion sources are useful in various fields [1]. One of the main fields of use is proton accelerator. These days, accelerators require increasingly higher beam power [2]. So the higher beam current is essential. Another area where proton ion sources are used is nuclear fusion. A neutral beam injector is used for plasma heating in the fusion field. It requires a high current beam of high energy too [3,4]. Neutron generators are also an important application of hydrogen (deuteron) ion sources [5] [6]. Deuteron-triton or deuteron-deuteron collisions are often used for neutron generation, so a high-performance deuteron beam ion source is essential. Thus, the critical performance required of the proton ion source is high beam power or current. On the other hand, it is also important to make more efficient beams. A high monatomic fraction beam is required for this reason. If molecular ions such as H_2^+ (or D_2^+) and H_3^+ (or D_3^+) are incident on the facilities, this will result in beam loss and may cause serious damage to the facility in some cases. And the energy of the single nucleon is divided to 1/2 and 1/3, the reaction rate of the target reaction is reduced.

Table 1.1 Hydrogen ion sources operated in diverse research fields.

Institute	Discharge Type	Beam current	Beam energy	Operation	Proton fraction	Application	Ref.
Seoul National University (Korea)	Helicon plasma (RF)	21 mA	35 keV	13.56 MHz / 1 kW RF, CW	94%	Proton accelerator, neutron generator	[5,6]
KAERI / KOMAC (Korea)	Microwave discharge	20 mA	50 keV	2.45 GHz / 400 W microwave	> 80%	Proton accelerator	[7,8]
NFRI / KSTAR (Korea)	Arc discharge	65 A	100 keV	75 V / 1030 A arc, > 10 s	80%	Nuclear fusion heating, NBI	[9]
JT-60U (Japan)	Arc discharge	40 A	100 keV	70 V / 700 A arc, 31 s	93%	Nuclear fusion heating, NBI	[10,11]
LBNL (USA)	Microwave discharge	100 mA	100 keV	2.45 GHZ / 450 W microwave, CW	95%	Neutron generator	[12]
U. C. Berkeley / LBNL (USA)	Penning discharge	20 μA	40 keV	600 – 800 V / 3 – 4 mA glow, CW	16.2%	Neutron generator	[13]
Sandia National Lab. / Zetatron (USA)	Penning discharge	> 100 mA	~ 120 keV	400 V / 2 A arc, pulse > 10 μs	< 10%	Neutron generator (sealed tube, portable)	[14,15]

Diverse hydrogen (proton or deuteron) ion sources operated in the research fields are listed in Table 1.1. Most of them has large beam current and high monatomic fraction. Basically high power resources can make dense plasma and it results in high beam current and high monatomic fraction. ECR ion sources or RF ion sources are popularly used these days, because of their high performance in the beam current and the monatomic fraction with a high-performance power supply even though they have complicated and expensive structure to fabricate.

Proton accelerators and tokamaks for nuclear fusion are very huge facilities, so the power resources for ion sources can be provided with almost no limits. However, neutron sources for neutron activation analysis tend to become smaller and portable and used mainly in situ. Sufficient power resources are difficult to be provided, and the choice of type and performance of the ion source are limited. Therefore, the ion sources for the neutron generators have much opportunity to be improved.

1.1.1 Neutron Activation Analysis and Neutron Generators [16-18]

In the non-destructive inspection field, X-ray or γ-ray is mainly used, and also in the case of mine detection, a metal detector is widely used. However, these methods are limited and require improvement. As an alternative to this, many researches are trying to develop non-destructive testing technology by neutron detection, Neutron Activation Analysis (NAA). It has advantage that it can separate the constituent elements of the target substance unlike the existing non-destructive inspection, and it is possible to inspect inside the metal container and the soil due to the high permeability of the neutron.

Neutron generators and neutron activation analyzers are needed to develop nondestructive testing equipment using neutrons. The neutron generator is a kind of radiation generator that generates neutrons by fusion reaction of hydrogen isotopes. The plasma is generated by discharging the hydrogen isotope gas, and the hydrogen isotope ions generated after the plasma is generated are accelerated to a high energy to collide with the target containing the hydrogen isotope. This is called a beam-target type neutron generator. In order to fabricate a high-yield neutron generator, the beam current and energy must be high. Particularly, the energy of the beam determines the size of the fusion reaction cross section and the maximum beam path length.

$$^{2}H + {}^{3}H \rightarrow {}^{4}He + n(14.1\ \text{MeV}) \quad (1.1)$$

$$^{2}H + {}^{2}H \rightarrow {}^{3}He + n(2.45\ \text{MeV}) \quad (1.2)$$

As shown in Figure 1.1 [19], the reaction cross-sectional area is maximum near 100 keV for the deuterium-tritium (D-T) fusion reaction and steadily increases to 3 MeV for the deuterium-deuterium (D-D) fusion reaction. The reaction cross-sectional area of the deuterium-tritium (D-T) fusion reaction is about 100 times larger on average. Therefore, it is important to develop a high-performance ion beam accelerator capable of supplying a large amount of high-energy beam current around 100 keV or over that for the production of a neutron generator for use in neutron activation analysis. If molecular ions are abundant, the energy of single nucleon is reduced to 1/2 or 1/3. This fusion is a reaction between nucleons, so high monatomic fraction also has big importance.

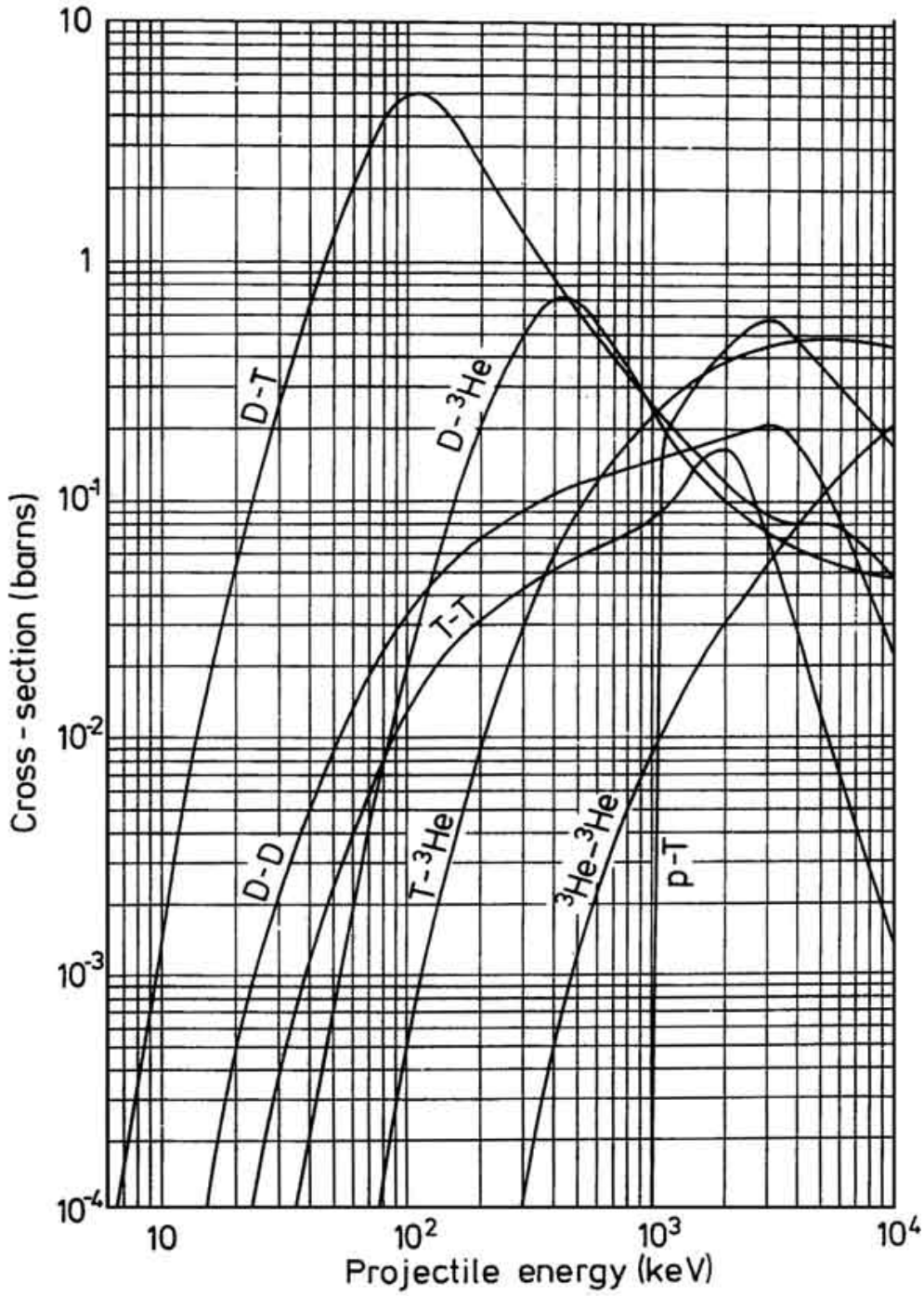

Figure 1.1 Fusion reaction cross-sections.

Another issue to consider when producing a neutron generator suitable for neutron activation analysis is the selection of neutron activation analysis. Neutron activation analysis techniques include Thermal Neutron Analysis (TNA), which are widely used in nuclear reactors, Prompt Gamma Neutron Activation Analysis (PGNAA), Pulsed Fast/Thermal Neutron Analysis (PFTNA), which is the most studied method for detecting illegal substances such as nuclear materials, explosives and drugs, and Pulse Fast Neutron Analysis (PFNA), etc. Among them, PFTNA puts a moderator between the neutron generator and the substance to be investigated, and investigates the object with both fast neutrons and thermal neutrons. Generally, the time width of fast neutron generation in the neutron generator is about 10 μs, and when operating at 10 kHz, the neutron generator is turned off for about 90 μs as shown in Figure 1.2 [16]. The thermal neutrons passing through the moderator are irradiated while the neutron generator is turned off. Since the fast neutrons and the thermal neutrons are generated with a slight time difference, it is possible to distinguish the gamma rays caused by the activation by the inactive scattering of the fast neutrons and the neutron capture reaction of the thermal neutrons.

In some cases, the neutron generator is operated at intervals of several minutes in order to diagnose the gamma ray of the half-life radiated nucleus having a short half-life within a few minutes. Therefore, PFTNA is the most suitable method for detecting search, explosives, unexploded ordnance, and landmines. To do this, the neutron generator must be operated in the pulse mode, and the pulse width is generally about 10 μs.

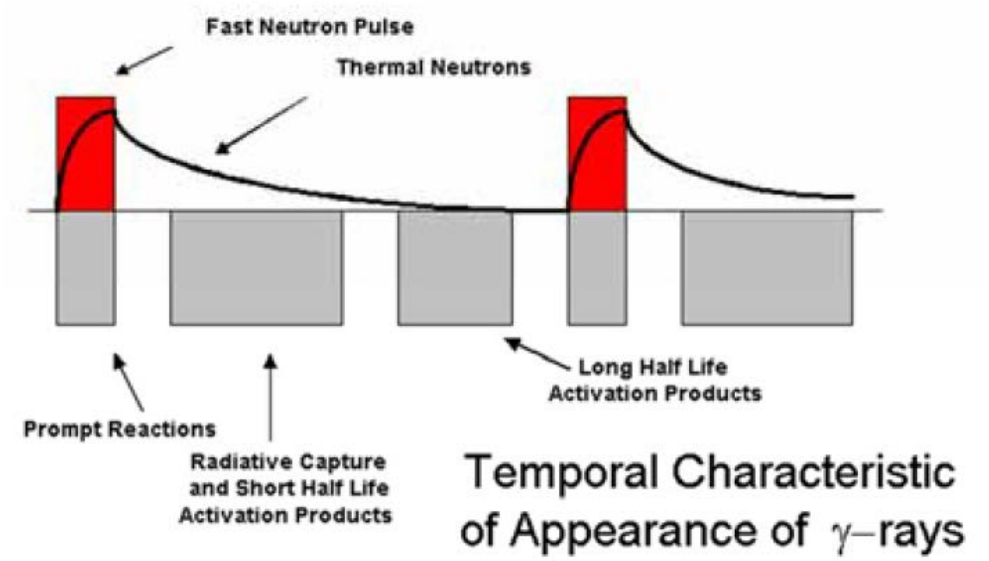

Figure 1.2 Time domains of information available from a pulsed NG. A typical pulse has a width of 1–10 μs, which is represented in red. Repetition rates vary for each application. The most commonly found are in the range of 100 Hz to 100 kHz.

Neutron generators are available in a variety of types and performances, from large-scale devices using accelerators to small-sized sealed tube type devices. However, when it is used for the purpose of detection in situ, the small size sealed tube type devices are used in consideration of the size of the entire system or suitability of the performance. The major performance of the neutron generator is 10^8 – 10^9 DT n/s and 10^6 – 10^7 DD n/s for neutron generation yield, beam energy is about 100 keV and beam current is about 0.1 A. The yield of neutron generators used in PFTNA is about 10^4 deuterium-tritium (D-T) neutrons for 10 μs.

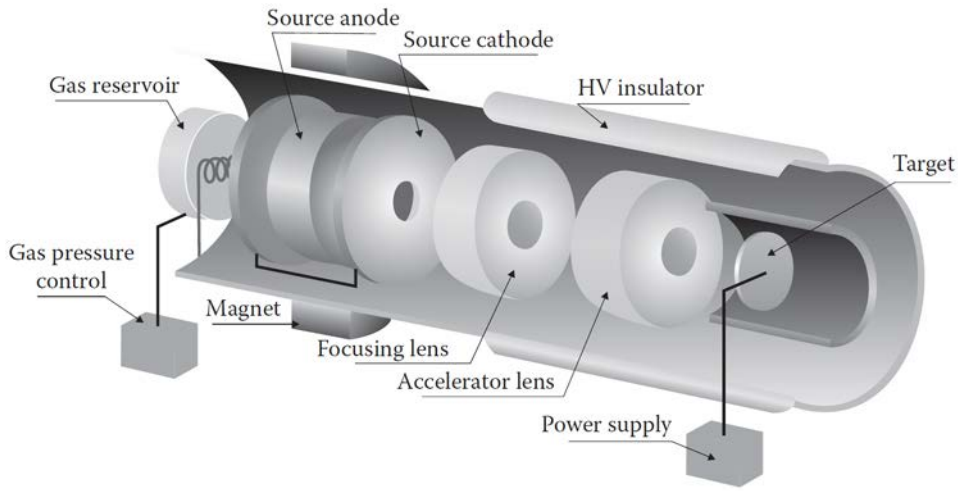

Figure 1.3 A schematic illustration of the internal structure of a compact neutron generator.

The neutron generator consists of an ion source that generates plasma and an acceleration stage that extracts and accelerates generated ions, and a target that generates neutrons like Figure 1.3 [17]. In the case of the ion source, Penning ion source is mainly used in commercial devices. Penning ion source is a plasma ion source based on DC discharge. It has a disadvantage in that impurities are generated due to the direct contact between the electrode and the plasma, and the ratio of the monatomic ion is low. However, the power source configuration is simple and the pulse mode operation is easy and the operating pressure is low. In RF and ECR (or microwave) plasma ion sources, discharge occurs in an insulator such as quartz, so there is less impurity generation and high ratio of single ion, but the beam current is low and power supply system is complex for a matching network of power system for RF or ECR (or microwave) plasma generation is required. Therefore, despite the disadvantages of that, small size neutron generators use Penning ion source.

1.1.2 Penning Ion Source

The Penning discharge was first invented by L. R. Maxwell in 1931. Penning ion source got its name from F. M. Penning who invented the Penning ionization vacuum gauge in 1937 [20]. A simplified schematic of Penning ion source is shown in Figure 1.4 [21]. Two cathodes are located at either end of a tubular anode within an axial magnetic field. Electrons emitted from either cathode are accelerated into the hollow anode as a beam, and a large fraction of them are trapped, axially by the electrostatic well and radially by the magnetic field. The primary beam electrons ionize the back ground gas to form the dense plasma from which the ion beam is to be extracted. The electrons eventually diffuse to the hollow anode, and the ions diffuse to the anode or accelerate to the cathodes [22].

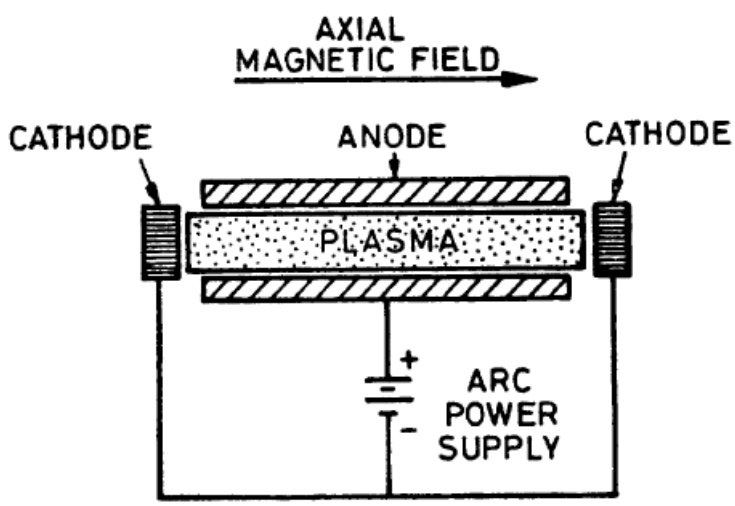

Figure 1.4 A simplified schematic diagram of Penning discharge source.

Schuurman was the first to categorize the Penning discharge modes and create their theory that was in reasonable agreement with measurements [23]. A modified form of Schuurman's classification is shown schematically in Figure 1.5 [24]. At low pressures (typically at $p < 10^{-4}$ Torr), the electron confinement time τ_e is much longer than the ion transit time τ_i so that the discharge is practically pure electron plasma. This low-pressure regime is divided into two regions (modes): the low magnetic field (LMF) mode and the high magnetic field (HMF) mode. In the LMF mode, the electron density in a Penning cell is small and the potential at the middle of the cell is close to the anode potential, as seen in Figure 1.5(a). The discharge current I_D is independent of the anode voltage V_a (Figure 1.5(b)). It is seen that the discharge current is proportional to the pressure ($v_{en} \propto p$) and to the square of the magnetic field. Not surprisingly, therefore, cold-cathode crossed-field gauges usually operate in the LMF mode. As the B-field is increased, the potential on the axis decreases to the cathode potential under the influence of electron space charge buildup; further increases in B lead to a transition to the HMF mode. The transition occurs when the radial potential drop becomes equal to the anode voltage. The discharge current reaches a maximum at the transition, as illustrated in Figure 1.5(b). This simple theory, based on the classical expression for the cross-field mobility of electrons, gives quite reasonable agreement with measurements in the LMF discharge mode; however, the agreement in the HMF mode is less satisfactory. In the HMF mode most of the applied voltage appears across a cylindrical electron sheath adjacent to the anode of a Penning cell (also referred to in the literature as an anode layer), as can be seen in Figure 1.5(a).

The physics of the electron sheath is still poorly understood. The sheath consists of magnetized electrons which cannot rapidly cross the magnetic field to go to the

anode. Approximately neutral plasma occupies the region near the axis at a potential close to the cathode potential and an electron density much below the sheath density. The HMF mode extends to very high B and is characterized by nonlinearity of I_D versus B characteristics (Figure 1.5(b)) accompanied, under certain conditions, by instabilities. In contrast to the LMF mode, the discharge current is an approximately linear function of the anode voltage, as seen in Figure 1.5(b).

At higher pressures ($p > 10^{-4}$ Torr), the discharge modes are all significantly affected by the presence of a positive space charge, since $\tau_i > \tau_e$. They are classified as the transition mode (TM), the HP mode and the GD mode, as shown in Figure 1.5(a). In the TM mode the positive space charge is somewhat small so that a significant part of the applied voltage still appears across the anode layer. At a certain pressure, however, the discharge can be sustained only if a cathode sheath is formed, and the discharge enters the HP mode. The Schuurman theory predicts the neutral density at the transition point (from the TM to the HP mode). With typical anode dimensions of a few centimeters, this neutral density corresponds to a gas pressure of about 10^{-4} Torr. Note that the HP mode is inherent to sputter magnetron sources since most of the discharge voltage drops across a thin ion sheath adjacent to the cathode. At sufficiently high pressures, when the electron mean-free path approaches the dimensions of the device, the magnetic field no longer has much effect and a GD occurs. At higher current densities, the discharge may transform into an arc. In this study, I will use mode between TM and HP, pressure range from sub-mTorr to several mTorr for plasma discharge and beam extraction [24].

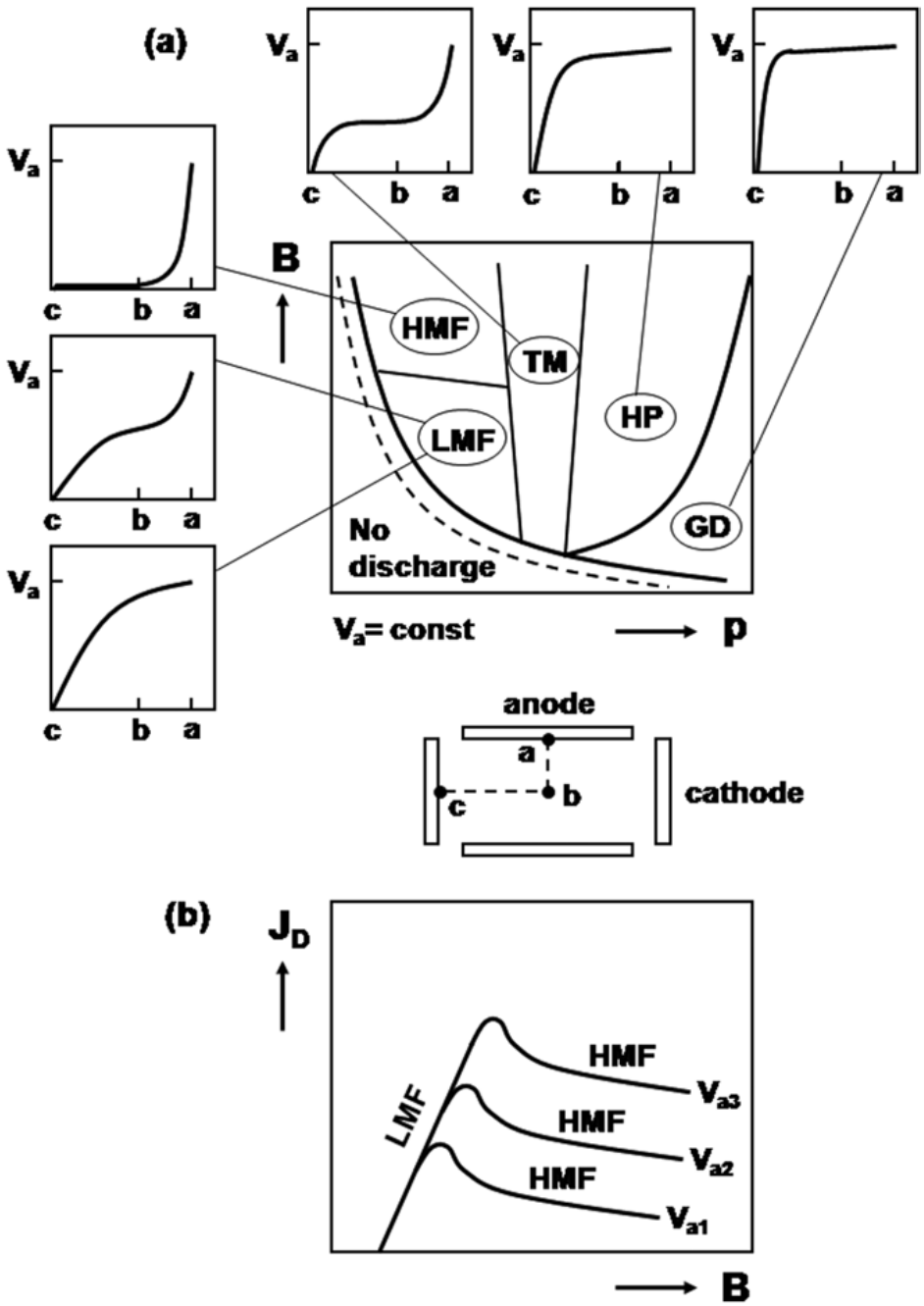

Figure 1.5 (a) Schematic representation of various Penning discharge regimes and their potential profiles. Dotted line represents discharge extinction curve. (b) Discharge current versus magnetic field with anode potential as parameter, $V_{a1} < V_{a2} < V_{a3}$.

The Penning discharge is divided into cold cathode discharge and hot cathode discharge depending on the cathode operation. The hot cathode discharge is a method in which one of the cathodes is heated by high current to release hot electrons from the cathode or heated indirectly by filament heating. Continuous arc discharge is possible because the hot electrons are continuously emitted from the hot cathode. It is actively used as an ion source for implantation process of semiconductor. In this case, a system such as a filament heating power source and a bias power source is required in addition to a power source for discharging between the cathode and the anode, which is not suitable for a portable sealing tube neutron generator. Cold cathode discharge is very simple. The anode and the cathodes are connected to each other by a DC power source, and a discharge is generated according to the current flowing through electrodes. Glow discharge occurs at low discharge current and continuous operation is possible. However, since the plasma density is low, a large beam current cannot be obtained. As the discharge current increases, the discharge goes to the arc discharge. Although a high plasma density can be obtained, the discharge is not continuously maintained. Our target device uses a short discharge of 10 μs, so it meets the target discharge. In this study, cold cathode Penning discharge is used for an ion source by pulsed operation.

1.2 Motivation and Scope of this Research

An example of a commercially produced sealed neutron tube is Zetatron, which is developed at Sandia National Lab. and distributed by Thermo Scientific, is shown in Figure 1.6 [14].

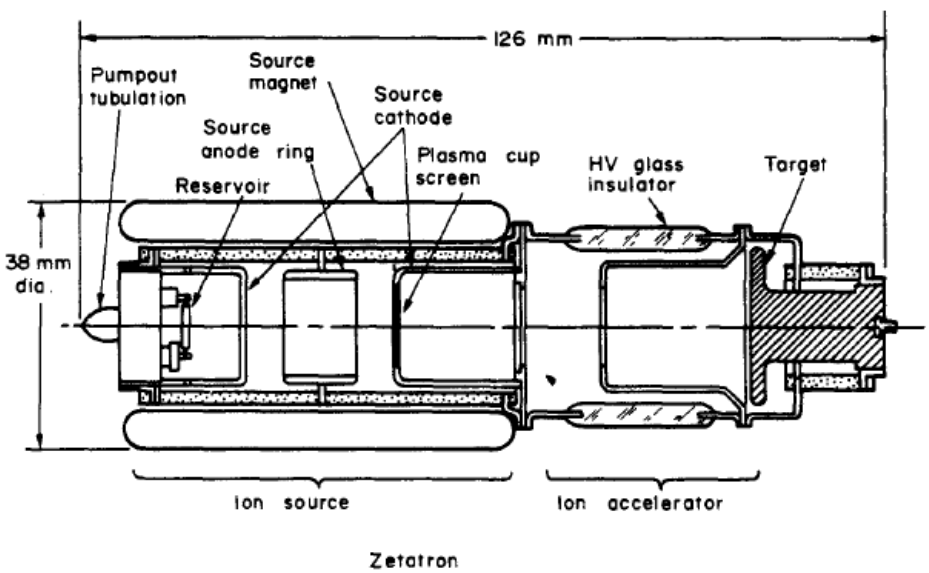

Figure 1.6 The Zetatron tube in cross section with tube structures and functions identified.

It is operated in about 2 A discharge current, and ion beam current over 100 mA can be extracted by 120 kV potential. It has high beam power, but monatomic fraction is poor. It is reported that D^+ fraction is about 5% [15]. It is due to low plasma density by low arc discharge current.

Since the sealing tube neutron source cannot replace internal components, the degradation of the components will determine the lifetime of the device. Factors limiting the lifetime of the device include He generation, a byproduct of the D-T

fusion reaction, consumption of deuterium reservoir, degradation of deuterium or tritium targets, and deposition on the inner insulator surface of the metal sputtered by the beam [14].

These factors are related to the extracted beam and neutron generation. Cathode degradation is another important lifetime-limiting factor inside the plasma sources. DC discharges are sustained by the emission of secondary electrons by ion bombardment on the cathode or by the thermal emission of electrons from the heated cathode. Particularly in cold cathode discharge, cathode degradation due to thermal electron emission is very large because electron emission is localized to a very small point (cathode spot). In order to minimize this influence, the discharge current cannot be greatly increased and the minimum discharge current must be maintained. This leads to a decrease in the monatomic fraction.

As described before, Penning ion source used for a portable sealed tube neutron source applicable to PFTNA can extract ion beam of 100 mA or more at an energy of about 100 keV. However, the monatomic fraction of the beam is less than 10% and the efficiency is low. Discharging with a high current can increase the monatomic fraction, but the operating conditions must be adjusted considering the lifetime of the sealed tube device.

This study aims to improve the performance of the cold cathode Penning ion source which can be applicable to the portable sealed tube neutron generator which can be used in PFTNA. Considering PFTNA, I operate with a pulse of 10 μs duration. The performance of the ion source is firstly a high beam current with a high energy, which is sufficient for the inherent performance of the Penning plasma source. The focus of this study is to improve the monatomic fraction of the beam. Considering the lifetime of the device, the amount of current applied to the cathode is limited.

Therefore, the operating conditions and the structure of the device that can achieve a high monatomic fraction at a low current discharge of several amperes are sought.

A theoretical consideration of hydrogen plasma and the model for calculating the hydrogen ion species fraction according to the plasma parameters by combining the reactions in the hydrogen plasma and the equations such as particle balance equations are presented in Chapter 2. In Chapter 3, new design of Penning ion source is presented. Hollow cathode is applied to basic Penning ion source. In Chapter 4, diagnostic method for measuring ion species fraction of shortly pulsed beam is presented. a time-of-flight mass analyzer is designed and fabricated. Chapter 5 shows the results and discussion about the measurement of the ion species fraction and the enhancement of monatomic fraction in new concept Penning ion source. Beam current measurement results are also presented. Finally, summary and conclusions are drawn in Chapter 6.

Chapter 2 Theoretical Backgrounds for Hydrogen Plasma Reaction and Ion Species Fraction

The production and loss of hydrogen ions in a hydrogen plasma is performed by connecting a number of reactions. When the state is in a steady state, the density values of atoms, the molecules and the ion species in the hydrogen plasma are in equilibrium, and the density values are obtained by combining the reaction rates of each reaction and the relational equations such as the particle balance equations. In this chapter, I investigate the changes of hydrogen ion species according to discharge condition and plasma parameters by combining hydrogen reactions, their reaction rates and relational expressions as a numerical modelling.

2.1 Hydrogen Reactions in Plasma

The reactions of hydrogen in a plasma is divided into volume reactions, which are caused by the collision of electrons, molecules, atoms and ions in the reaction volume, and surface reactions, in which atoms and ions are recombined in the wall of the vessel. The volume reactions considered in this study and its notation for the corresponding rate coefficients are as Table 2.1 [25,26]. Actually, there are more reactions in the hydrogen plasma such as the negative ion reactions and the reactions of vibrationally excited state of the molecule. However, the contribution of such reactions is known to be less than 10% [27], so these reactions are less effective in calculating the positive ion species fraction in this study and are not considered in this reaction list.

Table 2.1 List of volume reactions.

Reactions	**Rate coefficients** $< \sigma v >$
$H + e \rightarrow H^+ + 2e$	K_1
$H^+ + e \rightarrow H + h\nu$	K_2
$H_2 + e \rightarrow 2H + e$	K_3
$H_2 + e \rightarrow H_2^+ + 2e$	K_4
$H_2 + e \rightarrow H^+ + H + 2e$	K_5
$H_2^+ + e \rightarrow 2H^+ + 2e$	K_6
$H_2^+ + e \rightarrow H^+ + H + e$	K_7
$H_2^+ + e \rightarrow 2H$	K_8
$H_3^+ + e \rightarrow H_2 + H$	K_9
$H_3^+ + e \rightarrow H^+ + 2H + e$	K_{10}
$H_2^+ + H_2 \rightarrow H_3^+ + H$	K_{11}

Table 2.2 List of surface reactions.

Reactions	**Rate coefficients**
$H \xrightarrow{\text{(wall)}} \frac{1}{2}H_2$	$K_{12} = \gamma D_{eff}^H / \Lambda_{eff}^2$
$H^+ \xrightarrow{\text{(wall)}} H$	$K_{13} = /\tau_{H^+} = u_{B,H^+} A_{eff}/V$
$H_2^+ \xrightarrow{\text{(wall)}} H_2$	$K_{14} = 1/\sqrt{2}\tau_{H^+} = u_{B,H_2^+} A_{eff}/V$
$H_3^+ \xrightarrow{\text{(wall)}} H_2 + H$	$K_{15} = 1/\sqrt{3}\tau_{H^+} = u_{B,H_3^+} A_{eff}/V$

Table 2.2 is the list of surface reactions [25,28]. τ_{H^+} is the characteristic for ion wall loss, u_{B,H_x^+} is the Bohm velocity of the relevant positive ion, A_{eff} is an effective area. D_{eff}^{H} is the effective diffusion coefficient describing the superposition of free Knudsen diffusion and collisional diffusion processes, Λ_{eff}^2 is the effective diffusion length and γ is the wall recombination factor.

Figure 2.1 represents the change of reaction rate coefficients according to the electron temperature [29]. The reaction rate is calculated by integrating the cross-section with the electron energy distribution function. The reaction rates in Figure 2.1 are resulted in assumption of the Maxwellian distribution.

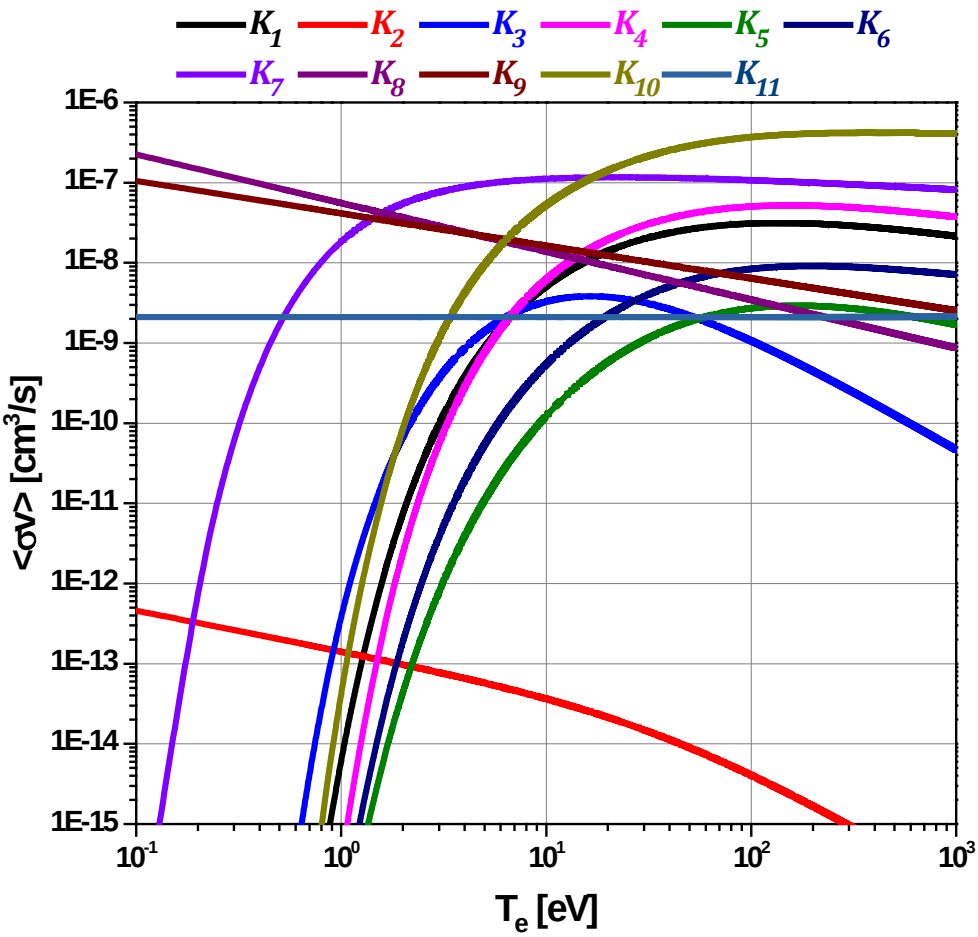

Figure 2.1 Reaction rate coefficients of 11 volume reactions listed in Table 2.1.

2.2 Equations for Numerical Model of Hydrogen Plasma

The ratios of the ion species can be calculated from the equations of particle balance in production and loss for each species of neutral particles and ions in the source plasma, i.e. atomic hydrogen H, molecular hydrogen H_2, atomic ion H^+ and molecular ions, H_2^+ and H_3^+ [25]. The variables for the modelling can be the plasma density, the electron temperature, the operating pressure, the wall materials, the geometrical structure of the vessel, etc. The most general form of the particle balance equation for the steady state of the discharge is shown in equation (2.1) where *p* and *d* indicate production and destruction processes for the *i*-th species, n_i is the species density, a_j is the number of particles of the species, k_j is the rate constant of the process, N_j is the number of the reactants involved, n_{jl} is the density of the *l*th reaction partner and k_r is rate constant for surface process reactions [30].

$$\frac{dn_i}{dt} = \sum_{j=1}^{N_p} a_j^p \, k_j^p \prod_{l=1}^{N_j^p} n_{jl}^p - \sum_{j=1}^{N_d} a_j^d \, k_j^d \prod_{l=1}^{N_j^{pd}} n_{jl}^d - k_r n_i = 0 \qquad (2.1)$$

Equations (2.2) through (2.5) are derived by equation (2.1) for each hydrogen ions and atom.

$$\mathrm{H}: a_2 n_{H^+} n_e + 2a_3 n_{H_2} n_e + a_5 n_{H_2} n_e + a_7 n_{H_2^+} n_e + 2a_8 n_{H_2^+} n_e + a_9 n_{H_3^+} n_e + 2a_{10} n_{H_3^+} n_e + a_{11} n_{H_2^+} n_{H_2} - a_1 n_H n_e - \gamma \frac{n_H}{T_1} = 0 \qquad (2.2)$$

$$\mathrm{H}^+: a_1 n_H n_e + a_5 n_{H_2} n_e + 2a_6 n_{H_2^+} n_e + a_7 n_{H_2^+} n_e + 2a_{10} n_{H_3^+} n_e - a_2 n_{H^+} n_e - \frac{n_{H^+}}{\tau_{H^+}} = 0 \qquad (2.3)$$

$$\mathrm{H}_2^+: a_4 n_{H_2} n_e - a_6 n_{H_2^+} n_e - a_7 n_{H_2^+} n_e - a_8 n_{H_2^+} n_e - a_{11} n_{H_2^+} n_{H_2} - \frac{n_{H_2^+}}{\tau_{H_2^+}} = 0 \qquad (2.4)$$

$$\mathrm{H}_3^+: a_{11} n_{H_2^+} n_{H_2} - a_9 n_{H_3^+} n_e - a_{10} n_{H_3^+} n_e - \frac{n_{H_3^+}}{\tau_{H_3^+}} = 0 \qquad (2.5)$$

In addition to Eq. (2.1), the conservation of total hydrogen atoms and the charge neutrality is used together to solve the problems.

$$n_{H_2} + \frac{1}{2}n_H + \frac{1}{2}n_{H^+} + n_{H_2^+} + \frac{3}{2}n_{H_3^+} = \frac{p}{k_B T_g} \tag{2.6}$$

$$n_{H^+} + n_{H_2^+} + n_{H_3^+} = n_e \tag{2.7}$$

Among the plasma parameters, the operating pressure and the electron temperature have the following relationship [31,32]

$$\frac{K_{iz}(T_e)}{u_B(T_e)} = \frac{1}{n_g d_{eff}} \tag{2.8}$$

Where K_{iz} is the rate constant for electron impact ionization, n_g is the neutral density and d_{eff} is the effective plasma size which is defined as the ratio of plasma volume *V* to effective area A_{eff}. n_g is a function of the operating pressure and K_{iz} and u_B are a function of the electron temperature. If the size of vessel is fixed, the operating pressure and the electron temperature have a correlated relation, especially near to inverse correlation.

For the specific conditions of a plasma density, an operating pressure (or an electron temperature), a wall recombination coefficient, and a geometric structure (volume and surface), the ion species fraction can be drawn by calculating the simultaneous equations from (2.1) to (2.8).

2.3 Ion Species Fraction by Hydrogen Model

The ion species fraction in the hydrogen plasma was calculated using the model established in Section 2.3. One of the variables was changed and the rest of them were fixed. The change of the ion species fraction according to the change of one condition was examined.

Figure 2.2 is the change of ion species fraction according to the wall recombination coefficient. The plasma density is set as 1×10^{12} cm^{-3}, the operating pressure 10 mTorr, and the electron temperature 5 eV. As shown in Figure 2.2, the monatomic fraction increases as the recombination coefficient decreases. However, the wall of Penning ion source is usually metal, and the recombination coefficient is fixed as about 0.1. So this change is not the focus of this study.

Figure 2.3 is the change of ion species fraction according to the operating pressure. The plasma density is set as 1×10^{12} cm^{-3} and the recombination coefficient 0.1. As shown in Figure 2.3, the electron temperature has an inverse correlation with the operating pressure. The monatomic fraction increases as the operating pressure decreases. The operating pressure is a controllable knob in the experiment by controlling the gas injection flow. And the Penning ion source is a source that can be operated at low pressure, which is advantageous for this condition.

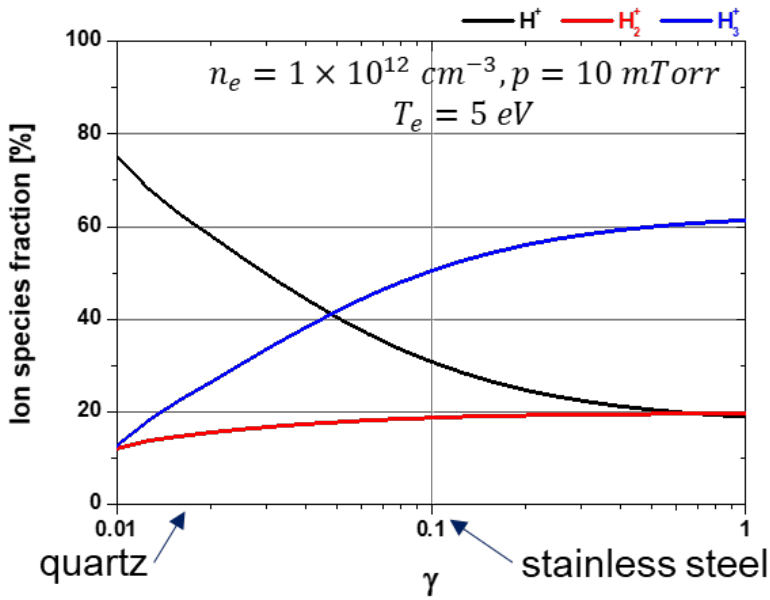

Figure 2.2 The change of ion species fraction by the wall recombination coefficient.

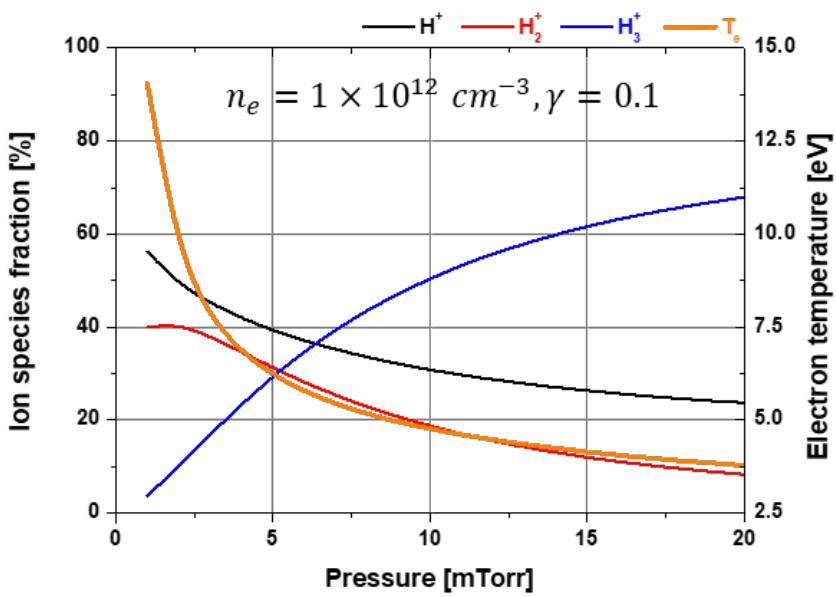

Figure 2.3 The change of ion species fraction by the operating pressure. The electron temperature has an inverse correlation with the operating pressure.

Figure 2.4 is the change of ion species fraction according to the electron temperature at a fixed operating pressure. The plasma density is set as 1×10^{12} cm^{-3}, the operating pressure 10 mTorr and the recombination coefficient 0.1. The electron temperature depends on the operating pressure, but other conditions can affect the change of the electron temperature such as the magnetic field, the geometric conditions, and so on. Therefore, the ion species fraction according to the change of the electron temperature at the fixed operating pressure was examined. As shown in Figure 2.4, the monatomic fraction increases slightly with increasing electron temperature at high electron temperature, but at low electron temperature, the monatomic fraction increases sharply at lower electron temperature. The overall tendency is that low electron temperature is required as a condition for a high monatomic fraction.

Figure 2.5 is the change of ion species fraction according to the plasma density. The recombination coefficient is set as 0.1, the operating pressure 10 mTorr, and the electron temperature 5 eV. As shown in Figure 2.5, the monatomic fraction increases as the plasma density increases. This is the main interest of the study. When the power is increased, the plasma density increases and the monatomic fraction increases. This is the reason why the monatomic fraction is increased by a high power resource of the RF ion source or the ECR ion source. In this study, however, I try to increase the plasma density and the monatomic fraction by constructing an efficient structure without applying additional power resources.

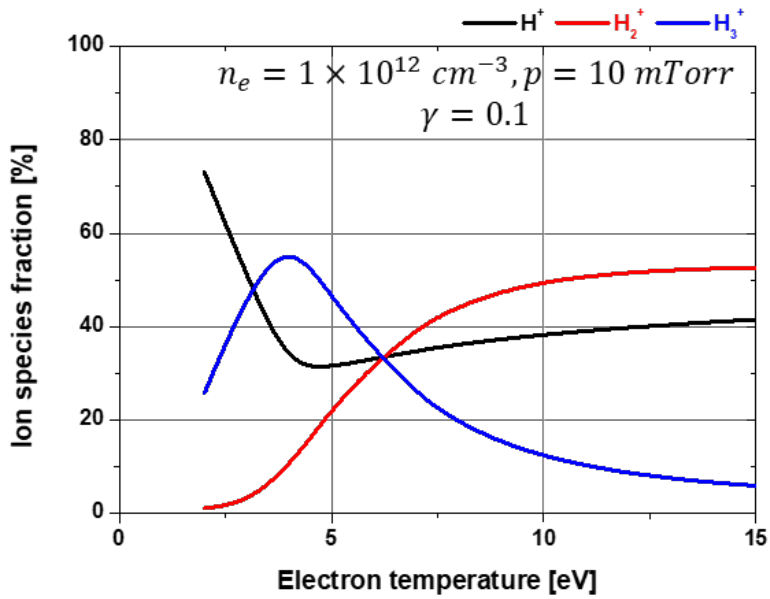

Figure 2.4 The change of ion species fraction by the electron temperature at a fixed operating pressure.

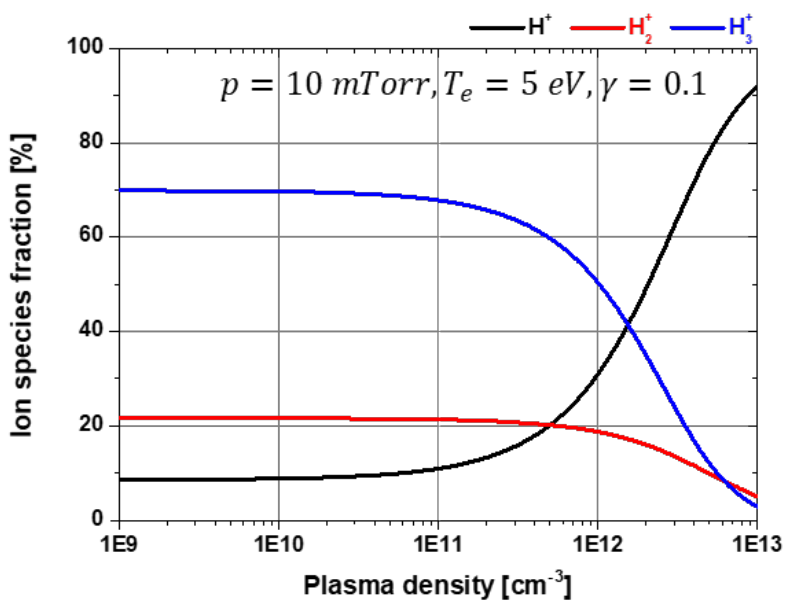

Figure 2.5 The change of ion species fraction by the plasma density.

In this section, a model for predicting the fraction of hydrogen ion species was constructed using the reactions in hydrogen plasma, and the change of ion species fraction according to plasma parameters and discharge conditions was examined. It was found that as the wall recombination coefficient is lower, the operating pressure is higher, the electron temperature is lower, and the plasma density is higher, the monatomic fraction increases. As mentioned earlier, in this study, I intend to construct an ion source with a structure that utilizes power efficiently in a conventional power system, rather than applying more power resources to increase the plasma density for a high monatomic fraction.

Chapter 3 Hollow Cathode Discharge

As stated in the previous section, it is advantageous to have high density and low electron temperature at low operating pressure to have a high monatomic fraction. The Penning ion source itself is an ion source that can have a high plasma density at low operating pressures. However, depending on the application, other discharge methods may be adopted and operated in a hybrid manner to obtain a higher plasma density. Typically, microwave ECR discharges using the same magnetic field are adopted [33-35]. In this case, although it shows excellent performance, it is necessary to have a separate expensive power system to apply microwave. This is not appropriate for the power system of the sealed tube neutron generator targeted in this study because of its increase in size. For the purpose of this study, the hybrid method should be in the form of a DC discharge that can use the same power source. A hollow cathode discharge can be a candidate.

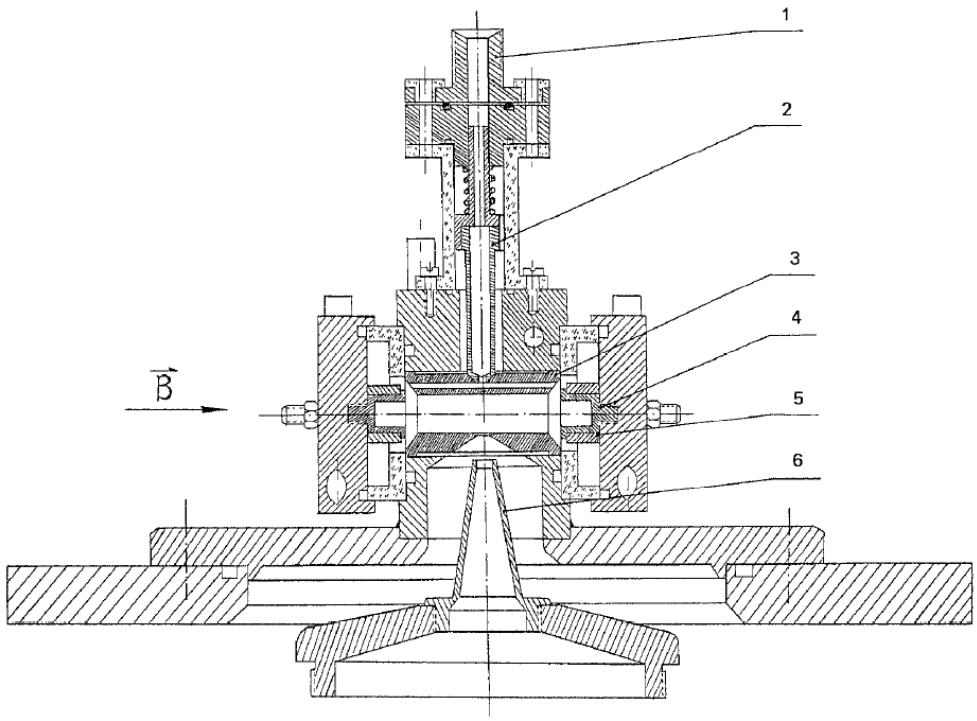

Figure 3.1 A cold-hollow-cathode lateral-extraction Penning ion source.

Figure 3.1 shows a structure in which a hollow cathode is used for both cathodes of the penning ion source and an extraction hole is formed in the anode to perform lateral extraction [36]. The application of this system is an ion implanter. The benefits of adopting a hollow cathode are an increase in the lifetime of the cathode and an improvement in the ion beam current. These two benefits can be also advantageous to the sealed tube neutron generator. However, the lateral extraction structure is difficult to use in sealed tube neutron generators usually using axial extraction.

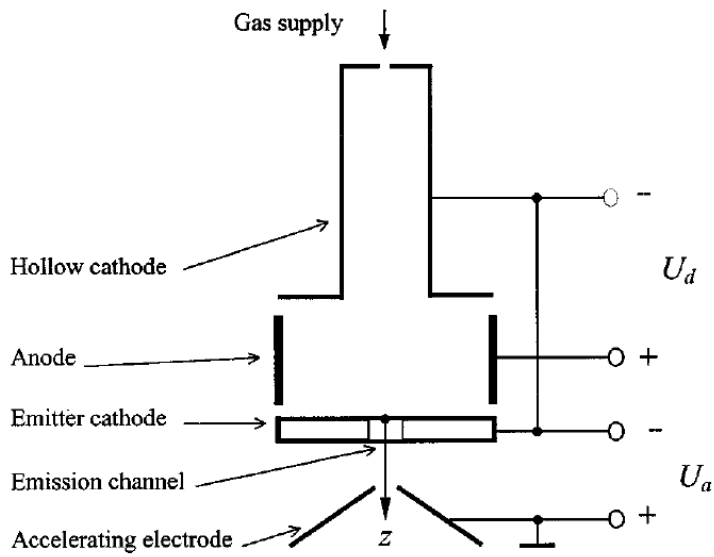

Figure 3.2 A plasma–cathode electron source.

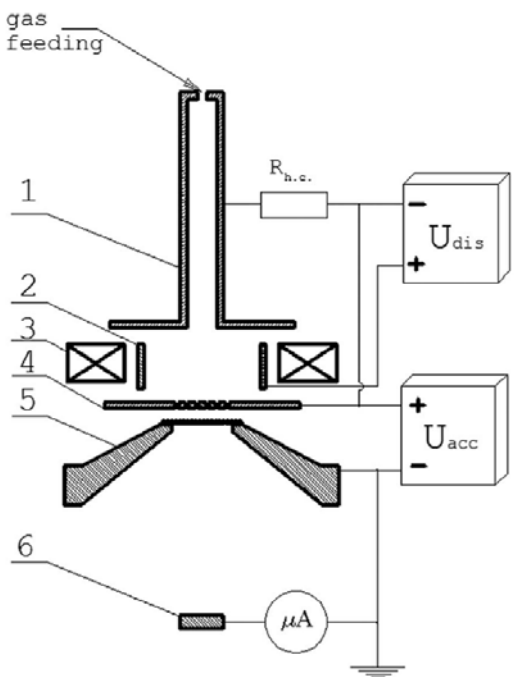

Figure 3.3 Low-energy dc ion source for low operating pressure.

Figure 3.2 [37] and Figure 3.3 [38] shows a axial extraction Penning ion source with a hollow cathode in opposite side of the extraction hole. The former is an electron source that can be used for welding etc., and the latter is designed as an ion source that can be used for versatile purposes. In both cases, as in the case of the previous lateral extraction ion source, the advantages of the increase of the cathode lifetime and the enhancement of the ion beam current were obtained.

Some examples presented here show that applying a hollow cathode has the potential to achieve the objective in this study.

3.1 Hollow Cathode Effect and Advantage of Hollow Cathode

The properties of hollow cathode (HC) glow discharges have been studied for many years. These discharges are traditionally widely used as light sources and active media for gas lasers [39]. Hollow cathodes were also used as thermionic emitters to produce electron beams. For electron beam source, cathode erosion is a severe problem because of cathode sputtering. However, the large area of the hollow cathode emitter prolonged the life of the delicate emitting surface at a given beam current. That is, hollow cathodes have been found to erode-less due to more diffuse current attachment [31,40]. This feature is also advantageous for a sealed tube neutron generator which cannot be replaced with a cathode.

Recent interest in HC discharges has been generated by the development of pseudo spark current switches, whose operation is determined by the hollow cathode effect (HCE). Owing to the HCE, the voltage in a HC discharge is lower at equal current density and the, current density is larger at a given voltage than for a similar direct current discharge with a planar cathode. As shown in Figure 3.4 [41], Paschen curve of a hollow cathode discharge has lower breakdown voltage than that of a glow discharge. This low voltage and high cathode current density discharge is advantageous for high plasma density. There are two main reasons for these differences [39].

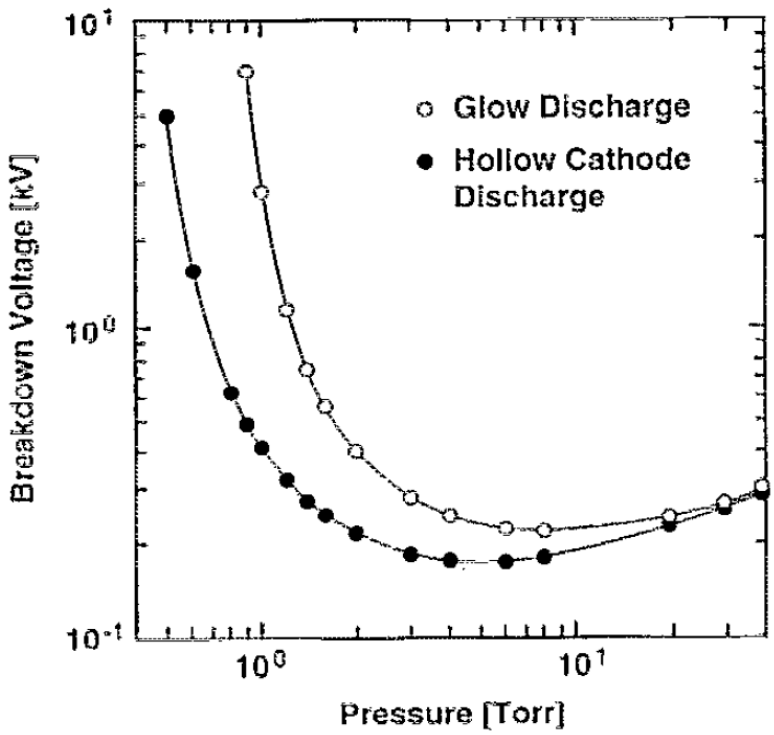

Figure 3.4 Paschen curves for a one-dimensional hollow cathode discharge and a glow discharge in helium.

The first is of geometric origin and is connected simply with reduction of charged particle losses in a closed space of a cavity. The HCE is observed under conditions when the fast electrons are far from equilibrium with the electric field. Being accelerated in the cathode sheath, they produce non-local ionization in the plasma where the electric field is weak, or even in the opposite sheath where the field is reversed. In a conventional planar discharge, some of these fast electrons would escape to the tube wall or to the anode taking away a considerable part of their energy. In a HC discharge, the fast electrons are electrostatically trapped and oscillate inside the cavity, expending all their energy for excitation and ionization of atoms. The ion losses are substantially reduced as well. In the absence of volume recombination, all the ions which are generated in the HC plasma are gathered by the cathode surface rather than by tube walls or by the anode. As a result, more γ -electrons are released in the secondary emission process, Thus, some of the specific features of hollow cathode discharges are due to reduced charged particle losses [39].

The second reason is connected with a higher efficiency of ionization in the HC cavity. The fast electrons, which perform oscillations between the opposite sides of the cathode sheath (the pendulum effect), create progeny electrons in ionization events. The pendulum effect by itself does not influence appreciably the generation of progeny electrons which are produced mainly in the low-energy range and, originating in the plasma, are not capable of producing further ionization. The ionization efficiency of the pendulum effect is due to the ability of oscillating electrons to create progeny electrons in the sheath. Being created in the sheath, the progeny electrons are accelerated in the intense sheath field and create further generations of electrons. The electron production in the sheath causes an exponential increase of the discharge current when a substantial fraction of ionization events

occurs in the sheaths. The difference between hear multiplication of electrons in the plasma and exponential multiplication in the sheath is primarily responsible for the HCE. For a given gas and the voltage drop in the sheath, the HCE takes place over a definite range of pressures p and the cathode cavity widths L. Near the upper boundary of pL, the fast electrons, after passing the plasma, reach the ionization threshold. Near the lower pL boundary, the pendulum effect is distinctly pronounced. The electrons perform a great number of bounces in the cavity before losing all their energy in collisions. The efficiency of the ionization is determined for these conditions by the ratio of sheath to gap lengths, d/L, which defines the probability of ionization in the sheath with respect to that in the plasma. The lower pressure cutoff can be explained by losses of fast electrons. Two kinds of losses can be distinguished. One is the escape of fast electrons through the output aperture of the cathode cavity and another is the absorption of γ -electrons by the opposite side of the cathode [39]. Figure 3.5 illustrates the pendulum effect [42]. In the hollow cathodes, electrons oscillate between the opposite sides of the cathodes.

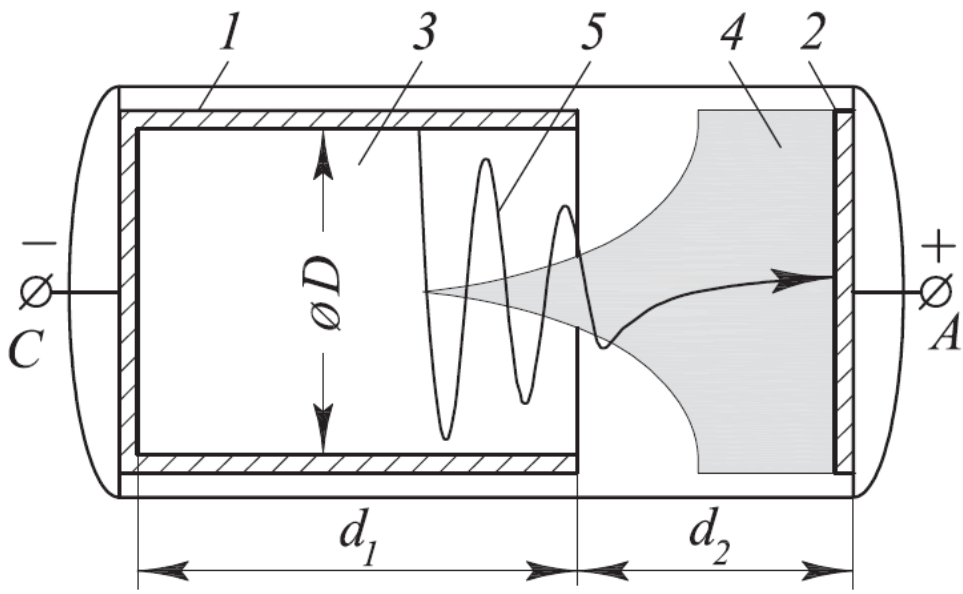

Figure 3.5 Classical hollow cathode discharge geometry illustrating transition from a high-voltage discharge into a glow discharge: 1-hollow cathode, 2-anode, 3-positive space charge, 4-plasma, 5-electron trajectory.

3.2 Penning Ion Source with Hollow Cathode

As explained in the previous sections, the advantages of the hollow cathode structure, that is, extending the lifetime of the cathode and increasing the plasma density, are useful for the sealed tube neutron generator application of the Penning ion source. In the application of the hollow cathode structure presented in the previous section, the ion source of Oks has an example of analyzing the pulsed discharge hydrogen ion beam. As shown in Figure 3.6 [43] a hollow cathode is adopted in opposite side of extraction hole. Hydrogen ion species fraction is measured by time-of-flight mass analyzer.

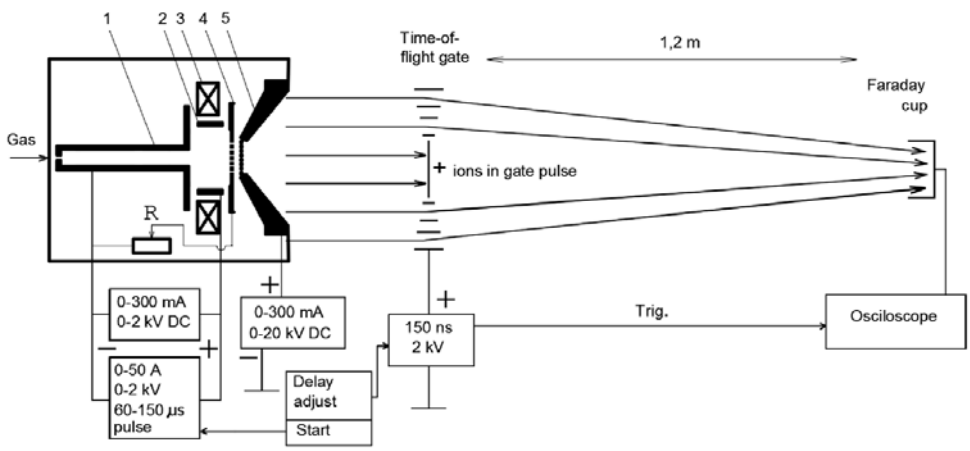

Figure 3.6 Schematic of the experimental setup for hydrogen pulse-operated Penning ion source with a hollow cathode in one side.

An example of mass spectrum is shown in Figure 3.7 [43]. In this experiment, changes in the ion species fraction were observed while adjusting the currents flowing through the hollow cathode and the reflector cathode (extraction side) using resistors.

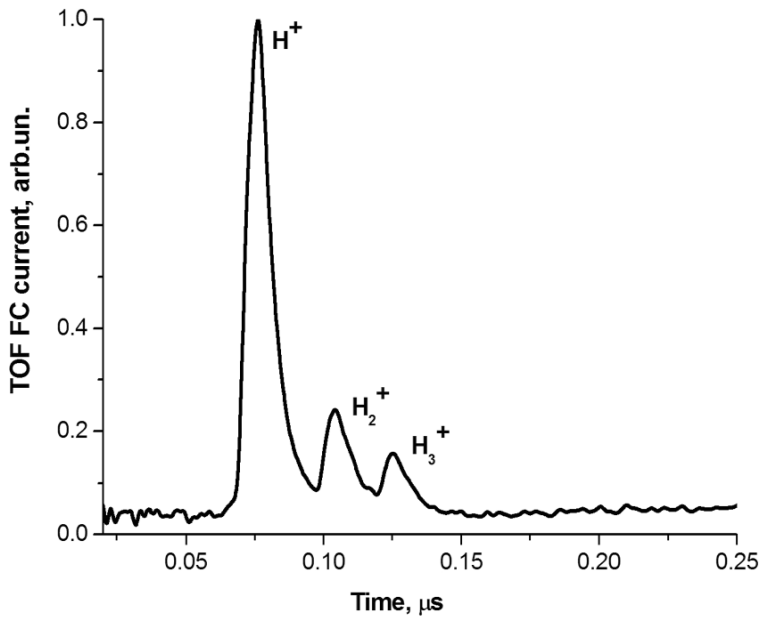

Figure 3.7 An example of mass spectrum by TOF mass analyzer.

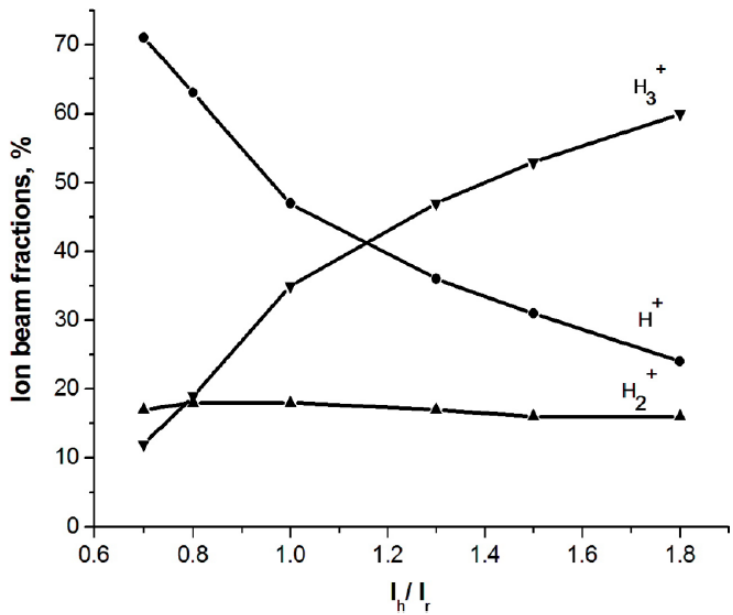

Figure 3.8 Ion species fractions vs the ratio between the hollow cathode current I_h and reflector cathode current I_r

Figure 3.8 [43] shows changes of ion species fractions according to the ration between the discharge current to the hollow cathode I_h and to the reflector cathode I_r. It is expected that when the discharge current flows to the hollow cathode, the plasma density increases and the monatomic fraction increases. In this case, on the contrary, the monatomic fraction decreases rapidly and H_3^+ molecular ions increase. This may be because the high-density plasma generated in the hollow cathode diffuses toward the extraction hole and the density decreases rapidly. So in the axial extraction Penning ion source, the hollow cathode in the opposite side of extraction hole do not work as desired as a high monatomic fraction with a hollow cathode.

As can be seen from the study above, if a hollow cathode is applied to improve the monatomic fraction, the hollow cathode has to be on the side of the beam extraction. Thus, as shown in Figure 3.9, I propose a design to convert both cathodes to a hollow cathode structure in the general Penning ion source on the left. Although it is possible to adopt a hollow cathode only for the beam extraction side, repeated experiments have shown that the discharge is stable when the ion source is symmetrical, and a hollow cathode is adopted for the opposite cathode too. This concept is similar to the lateral extraction ion source for the ion implanter shown in this chapter, but it can extract the beam directly from high density plasma discharged from the hollow cathode. And the structure of a sealed tube neutron generator is different from that structure because the beam has to be extracted axially.

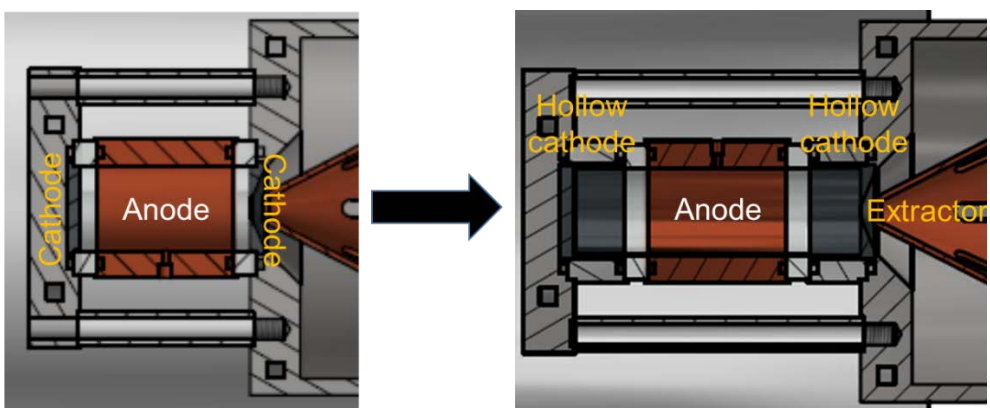

Figure 3.9 A new concept of Penning ion source adopting the hollow cathodes.

Chapter 4 Time-of-flight Mass Analyzer

In order to verify the improvement of the monatomic fraction of the new structure Penning ion source, a diagnostic system is required. To measure the ion species fraction, the mass analyzer should be used, which is measuring the mass-to-charge ratio (m/q). A typical method for measuring m/q is to use magnetic field [44]. This method has merits in its high resolution and accurate analysis, but the inductance of the magnets limits the scan speed in which the field strength is changed. Because of the limit of scan speed, a magnetic mass analyzer cannot measure mass spectrum of ion beam that is maintained in a short period. Our target system operates in a very short duration, ~10 μs. So another solution is required. The time-of-flight (TOF) mass analysis can be an alternative method [44]. TOF method uses the velocity difference of ions that have different m/q states. This method is widely used in chemical analysis such as MALDI-TOF mass spectrometry [45]. For an elaborate chemical analysis, the ion mirror (reflectron) or the orthogonal acceleration TOF is mainly used [46]. However, for the development of ion sources, the early TOF mass analyzer, which operates with gating and detection of ion packets in a linear configuration, is still used because of its simplicity and low cost, in spite of its low sensitivity. In 1980s, a TOF system with a gating device composed of concentric annular plates was proposed to increase the ion collection efficiency and thus improve the signal-to-noise ratio (SNR) [47]. Due to its good performance, this type of TOF mass analyzer has been actively used to measure the mass and charge states of various kinds of ion sources [43,47-50]. However, despite the significant improvement in SNR, I recognize that the electric potential near the gating device could be distorted due to unbalanced gate bias and geometry of gate electrodes. In

this study, I have changed the way of applying the voltage on the electrodes of the gating device and improved the structure of electrodes to minimize potential distortion near the gating device. These improvements minimize the ion loss during the transport to a Faraday cup and thus increase the SNR significantly.

4.1 Principle of Operation

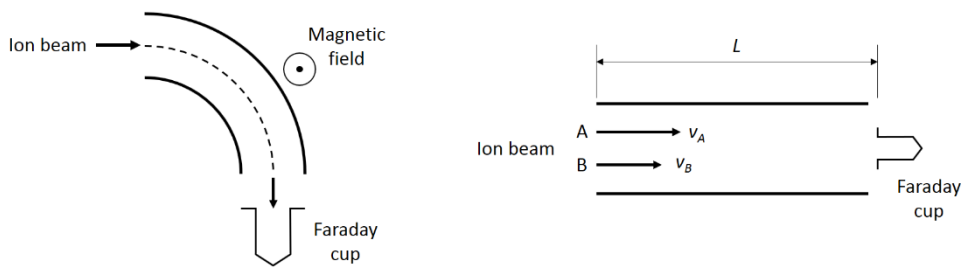

(a) (b)

Figure 4.1 Brief diagram of (a) the magnetic field type mass analyzer and (b) the time-of-flight mass analyzer.

Figure 4.1 and Eq. (4.1), (4.2) briefly show the principle of a magnetic type mass analyzer and a time-of-flight mass analyzer. A magnetic field type mass analyzer utilizes the property that the ion beam is deflected by the Lorentz force as it passes through the magnetic field. The mass-to-charge ratio is proportional to the square of magnetic field strength as shown in Eq. (4.1). V_{acc} is the acceleration potential of ion beam and R is the radius of the ion beam path.

$$\frac{m}{q} = \frac{R^2}{2V_{acc}} B^2 \tag{4.1}$$

Since the magnetic field strength through which ion beam can enter the detector differs depending on the mass-to-charge ratio, it must be measured by changing the magnetic field with time. So it is difficult to apply it to the ion source in pulsed operation in which the discharged occurs for a short period of time. The time-of-flight type mass analyzer uses the principle that the traveling time of ion beam in a drift tube of a certain length depends on the mass-to-mass ratio as shown in Eq. (4.2). *L* is the drift length of ion beam.

$$\frac{m}{q} = \frac{2V_{acc}}{L^2} t^2 \tag{4.2}$$

In order to distinguish the beam signals by the ion mass-to-charge ratio, the time during which the beams are supplied must be smaller than the time difference between arrivals of ion beams with each mass-to-charge ratio.

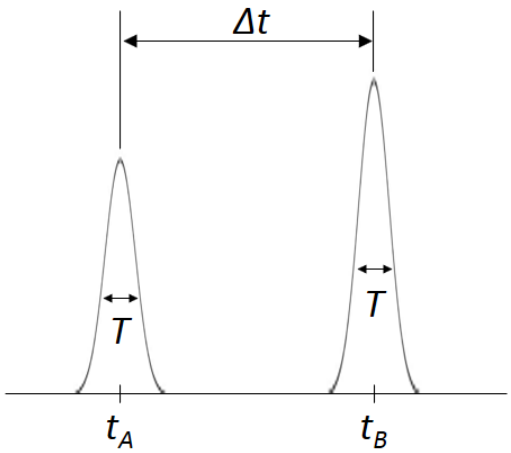

Figure 4.2 Resolution of ion beam signals.

As shown in Figure 4.2, in order to distinguish the signals of ion beam A and B, T must be much smaller than Δt. In general, Δt is hundreds of nanoseconds to microseconds, so T should be about several hundred nanoseconds. It is difficult to operate plasma discharge or beam extraction for such a short period of time, and it is unclear whether the characteristics of the plasma or the beam are maintained consistently. To solve this problem, the deflection gate is employed. It is a device that opens the gate for a very short time and chop the beam into very short pulse beam while the beam is being extracted. So the beams which enters Faraday cup can be distinguished by the mass-to-charge ratio. The basic concept is shown in Figure 4.3. The deflection gate consists of several pairs of concentric metal plates [47,49]. $V_{def,+/-}$ is applied for a short time (T) between the metal plates, causing the beam to be deflected due to the formed electric field and to be detected in the Faraday cup. The ion beam deflection angle θ is given by Eq. (4.3). d is the gap between electrodes of the deflection gate.

$$\theta \sim \frac{V_{def} L}{2 V_{acc} d} \tag{4.3}$$

At the center of the deflecting gate, there is a blocking plate that prevents the beam from flying to the detector when the gate is closed. As a result, the ion beam signals can be separated by the mass-to-charge ratio and the signals are shown as peaks in the plane of time vs. beam current.

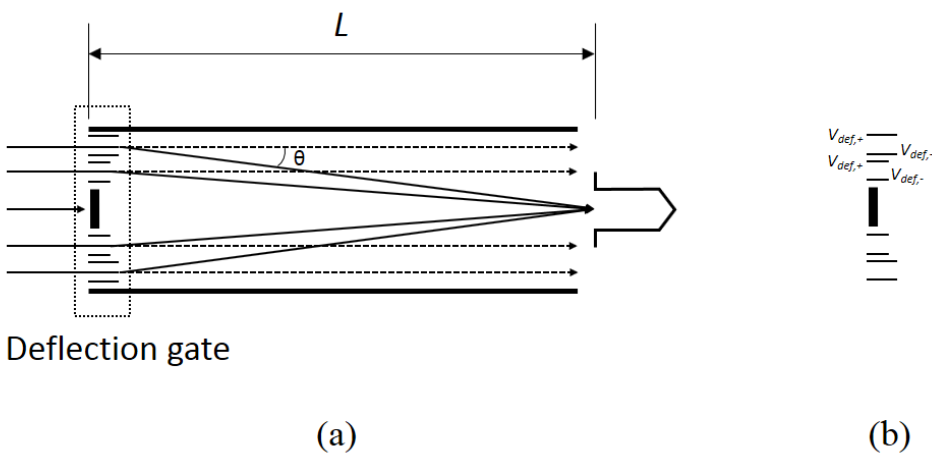

Figure 4.3 (a) Principle of deflection gate and (b) voltage assignment to concentric electrodes.

4.2 Design and Fabrication

The experimental apparatus consisting of an ion source and a TOF system is shown in Figure 4.4. A pulse-operated cold-cathode Penning ion source is used to generate hydrogen ion beam. The hydrogen plasma is produced by applying discharge initiation voltage (V_{disch}) of ~3 kV during ~100 μs. The discharge current is adjusted by changing the value of a current limiting resistor (R_{lim}). An axial magnetic field of 35 mT is supplied by a solenoid magnet surrounding the ion source. Hydrogen ion beam is extracted from 3 mm dia. hole with an acceleration voltage (V_{acc}) of ~10 kV.

A TOF system is attached to the ion source in order to identify ion species spectrum generated in the hydrogen plasma. It consists of a long drift chamber, a gating device, and a Faraday cup, as shown in Figure 4.4. The gating device is installed 45 cm apart from the extraction hole. The extracted ion beam is sampled in a short pulse of ~200 ns through the gating device. The sampled ion beam flies through a drift chamber of 1.5 m in length. To minimize beam loss due to collisions with residual gas in the drift chamber, another turbo-molecular pump is installed in the ion beam drift region. A Faraday cup is attached at the end of the drift chamber in order to collect ion beam. The current signal is converted to the voltage signal through the measuring resistance R_{meas} and the data are recorded by an oscilloscope. The mass spectrum of ion beam is obtained by distinguishing the arrival time of each species at the Faraday cup according to the ion mass-to-charge ratio, and counting relative amount of ion species.

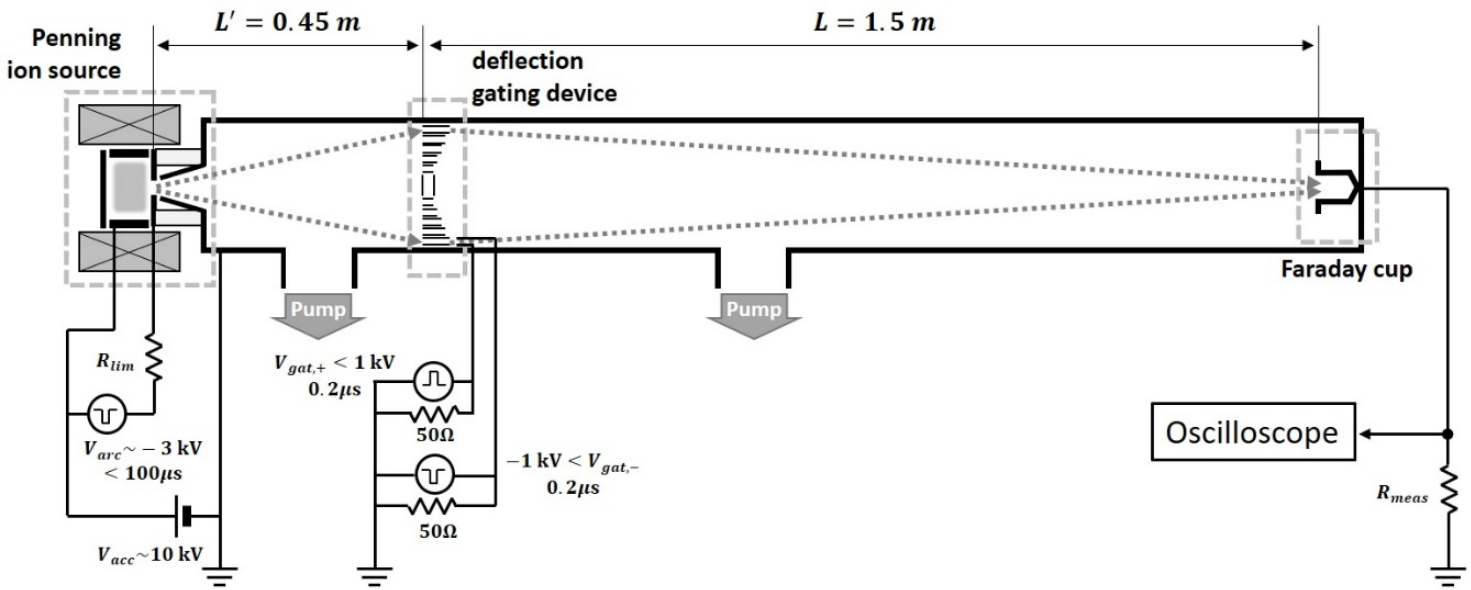

Figure 4.4 The experimental apparatus consisting of an ion source and a TOF system.

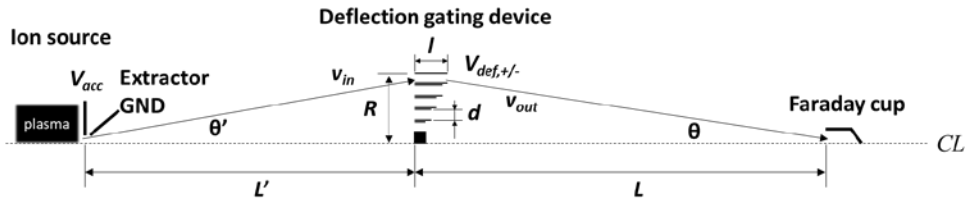

Figure 4.5 Design parameters of the time-of-flight mass analyzer.

The trajectory of the beam extracted from the ion source to the Faraday cup through the deflection gating device can be calculated using Equation (4.4) to (4.10) with the parameters in Figure 4.5.

$$v_{in} = \sqrt{\frac{2qV_{acc}}{m}} \tag{4.4}$$

$$v_{in,x} = v_{in}\cos\theta' = \frac{L'}{\sqrt{L'^2 + R^2}}v_{in} \tag{4.5}$$

$$v_{in,y} = v_{in}\sin\theta' = \frac{R}{\sqrt{L'^2 + R^2}}v_{in} \tag{4.6}$$

$$v_{out,x} = v_{in,x} \tag{4.7}$$

$$v_{out,y} = v_{in,y} - at' = v_{in,y} - \frac{qV_{def}l}{mv_{in,x}d} \tag{4.8}$$

$$t' = \frac{l}{v_{in,x}} \tag{4.9}$$

$$\tan\theta = \frac{R}{L} = -\frac{v_{out,y}}{v_{out,x}} = \frac{L'^2 + R^2}{L'^2}\frac{V_{def}l}{2V_{acc}d} - \frac{R}{L'} \tag{4.10}$$

Figure 4.6 shows a cross-sectional view of a gating device and its electrical arrangement. Considering the size of the vacuum drift chamber, the outer diameter of the gate device is set to be 17 cm. At the center, a blocking plate of 30 mm in diameter is located to prevent the ion beams from directing to the detector when the gating pulse is not applied. The gating device is designed to have five concentric apertures ($A_1 - A_5$). Each aperture has two electrodes separated by a gap *d* of 12 mm. When the gating voltage pulse of V_{gat} is applied between the two electrodes, the ion beams passing through the apertures are deflected by the electric field ($E = V_{gat}/d$), and finally collected in the Faraday cup.

The performance of TOF system depends mostly on the deflection of ion beams at each aperture to a single focal point where the Faraday cup is located. In order to have a single focal point, ion beam passing through the outer aperture have to be deflected with a bigger angle than that through the inner aperture. Therefore, the length of electrode pair of the outer aperture (l_n) is longer than that of an inner aperture (l_{n-1}). The length of electrode (l_n) can be simply described by

$$l_n = \frac{2V_{acc}d}{V_{gat}} \cdot R_n \cdot \frac{1/L + 1/L'}{1 + {R_n}^2/{L'}^2} \tag{4.11}$$

where, R_n is the radius of the center line of the *n*-th concentric aperture A_n with the electrode gap *d*. *L'* and *L* are the distances among the extraction electrode, the gating device, and the Faraday cup, as depicted in Figure 4.4. *L'* and *L* are 0.45 m and 1.5 m, respectively.

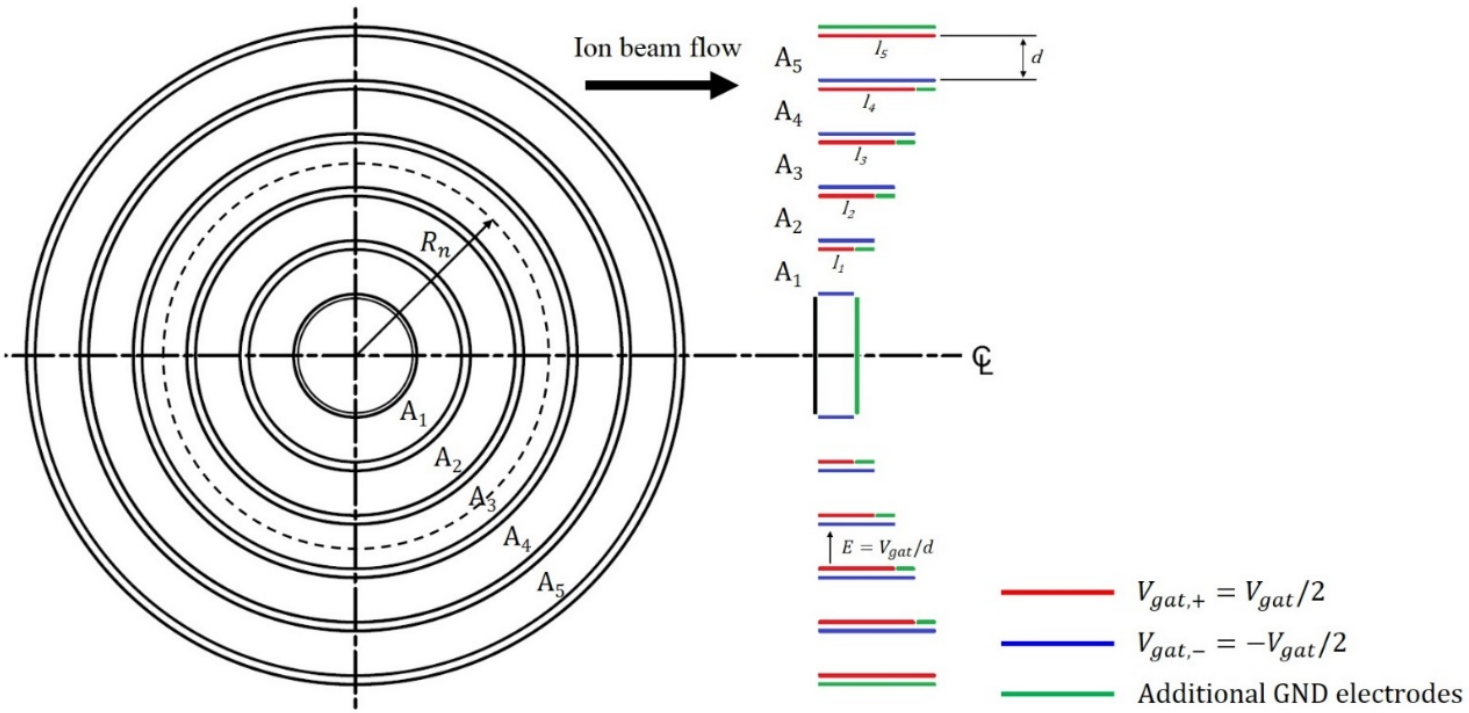

Figure 4.6 Cross-sectional view of the gating device and its electrical arrangement.

For the V_{acc} of 10 kV and V_{gat} of 1700 V, the length of each electrode (l_n) is calculated as 9 mm, 14 mm, 20 mm, 25 mm, and 30 mm for R_n, 22 mm, 36 mm, 50 mm, 64 mm, and 78 mm.

In the design of the gating device, two important advances are made for minimizing field distortion and thus improving ion collection efficiency; one is the application of a bipolar gating pulse on deflecting electrodes and the other is the addition of ground electrodes at the exiting edges of deflecting electrodes. In the previous work [47,49], a unipolar pulse was applied to make an electric field E (= V_{gat}/d) in the aperture, i.e., a ground potential was applied to the inner electrode of an aperture, and a potential of V_{gat} was applied to the outer electrode. In this case, ion beam feels the averaged potential of $V_{gat}/2$ before entering the aperture (see Figure 4.7(a)), so the ion beam energy is reduced and the deflection condition in the aperture is disturbed, resulting in the loss of ion beam. To avoid this problem, I apply the potential $V_{gat}/2$ to the outer electrode, and the potential $-V_{gat}/2$ to the inner electrode to make the electric field V_{gat}/d. Utilization of the bipolar pulse on the deflecting electrodes greatly reduces the leakage electric field which affects the trajectory of ion beams before entering the gating device, as shown in Figure 4.7(b). Further improvement is accomplished by using additional ground electrodes at the exiting edges of deflecting electrodes. In principle, the negative potential electrode of the outer aperture is always longer than the positive potential electrode of the adjacent inner aperture. Therefore, the negative potential electrode protrudes from the inner positive potential electrodes in downstream side of the ion beam flow. The negative potential from the protruded electrode affects the potential structure and makes a potential dip in the downstream side. To minimize field distortion by this, I add ground electrodes at the exiting edge of deflecting electrodes as depicted in Figure

4.6. Moreover, an additional ground electrode is attached to the outside the outermost electrode in order to shield the electric field generated by the outermost positive potential. From the electrostatic analysis using a commercial simulation package, the influence of both bipolar operation and ground electrodes on the leakage electric field near the gating device is clearly verified in Figure 4.7. The photographs of totally fabricated system are shown in Figure 4.8.

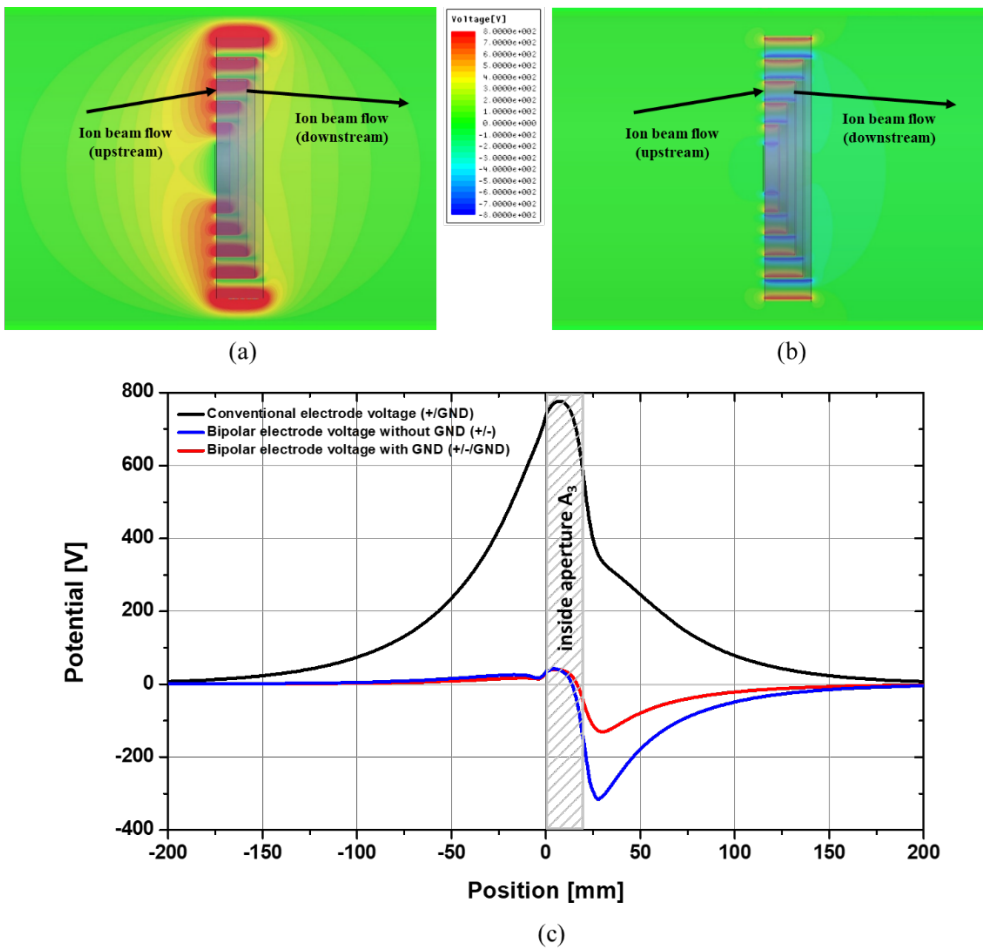

Figure 4.7 Comparison of the electric potential distribution between the conventional method and the new method adopted in this paper; (a) conventional method (inner electrode: ground, outer electrode: +1500 V), (b) new method (inner electrode: -750 V, outer electrode: +750 V, with additional ground electrodes), (c) variation of the electric potential along the beam path from the ion source to the Faraday cup through the aperture A_3.

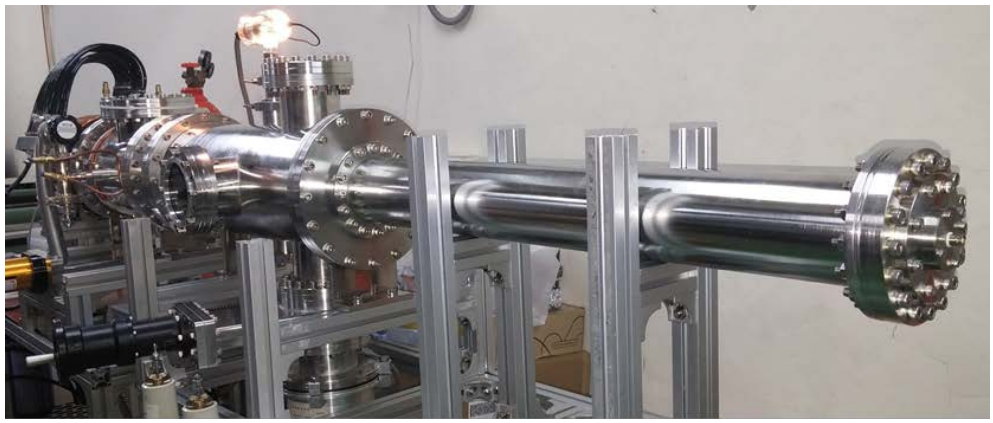

(a)

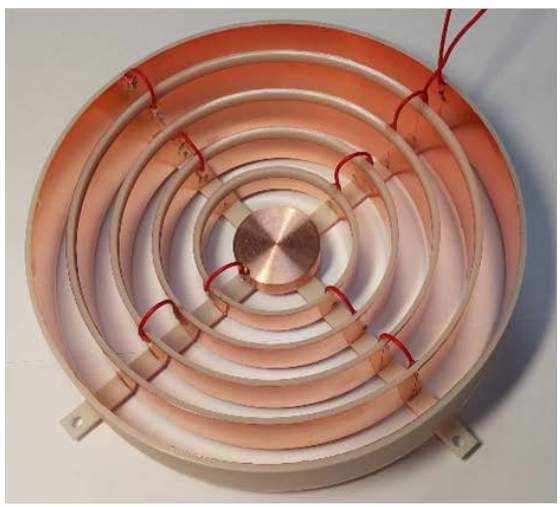

(b)

(c)

Figure 4.8 The photos of the fabricated system; (a) total system with ion source and TOF, (b) gating device, (c) TOF system.

4.3 Operation Test

Figure 4.9 shows a typical Faraday cup signal (upper panel) and a bipolar gating voltage (lower panel) obtained by the newly developed TOF mass analyzing system for the measurements of the hydrogen ion species fraction from a Penning ion source. In this case, the hydrogen ion beam is extracted from the Penning source operating at 10 mTorr with a discharge current of 17 A. The extraction voltage is about 10 kV. The FWHM of a bipolar gate pulse with -750 V / + 750 V is around 210 ns, which is shorter than the difference in arrival times among the hydrogen species to be measured. I can clearly resolve the ion species according to the arrival time as shown in Fig. 4. Note that the measured arrival times, 1.12 μs for H^+, 1.56 μs H_2^+, and 1.90 μs for H_3^+ are almost the same as the calculated ones for the ion beam energy of 10 keV.

Figure 4.10(a) compares the ion beam signal obtained from the improved gating device and the signal from the conventional one. In the conventional method, the inner electrode of a concentric aperture is grounded and the ion beam is sampled by applying 1500 V to the outer electrode. Whereas, the inner electrode is set to -750 V, the outer one to +750 V, and the additional electrodes are grounded for the improved gating device. I clearly observe that the beam current signal is increased by ~50% compared to the conventional one, when the improved gating device developed in this paper is used. On the other hand, the base noise is equal to about ± 0.06 peak-to-peak in the normalized beam current value regardless of the gating device type. Thus, it is concluded that the SNR is improved by about 50% because the signal value is improved by about 50% at the same noise level. Figure 4.10(b) shows the averages and errors of the peak values of ion species signals measured 50 times under

the same condition, indicating excellent measurement repeatability of hydrogen ion species using the present TOF system.

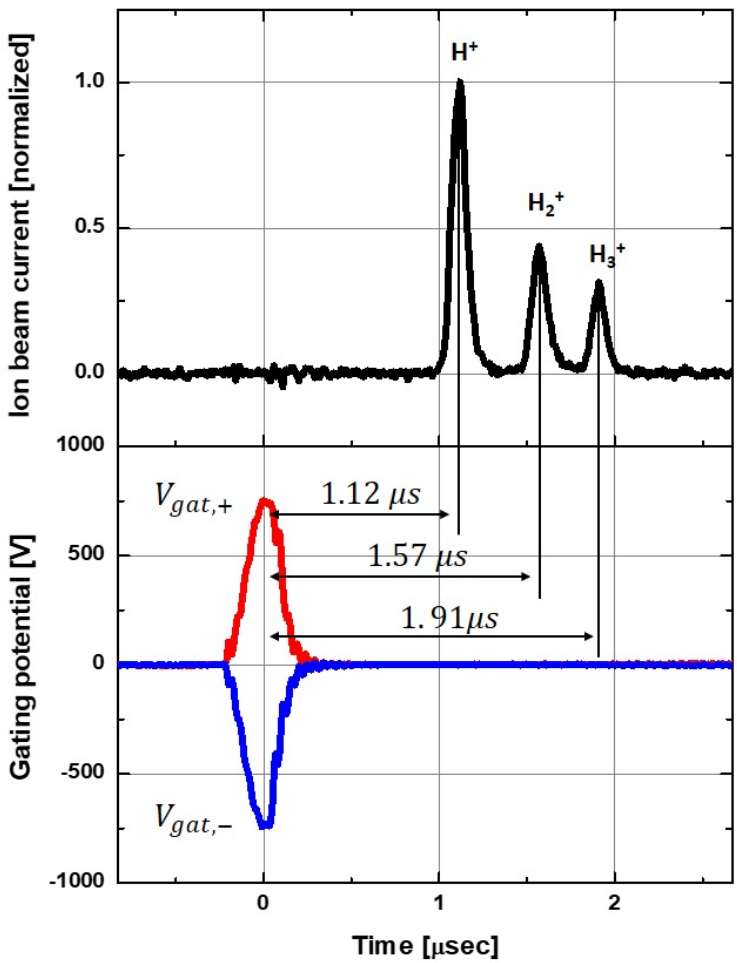

Figure 4.9 A typical Faraday cup signal (upper panel) and a bipolar gating voltage (lower panel) obtained by the newly developed TOF mass analyzing system.

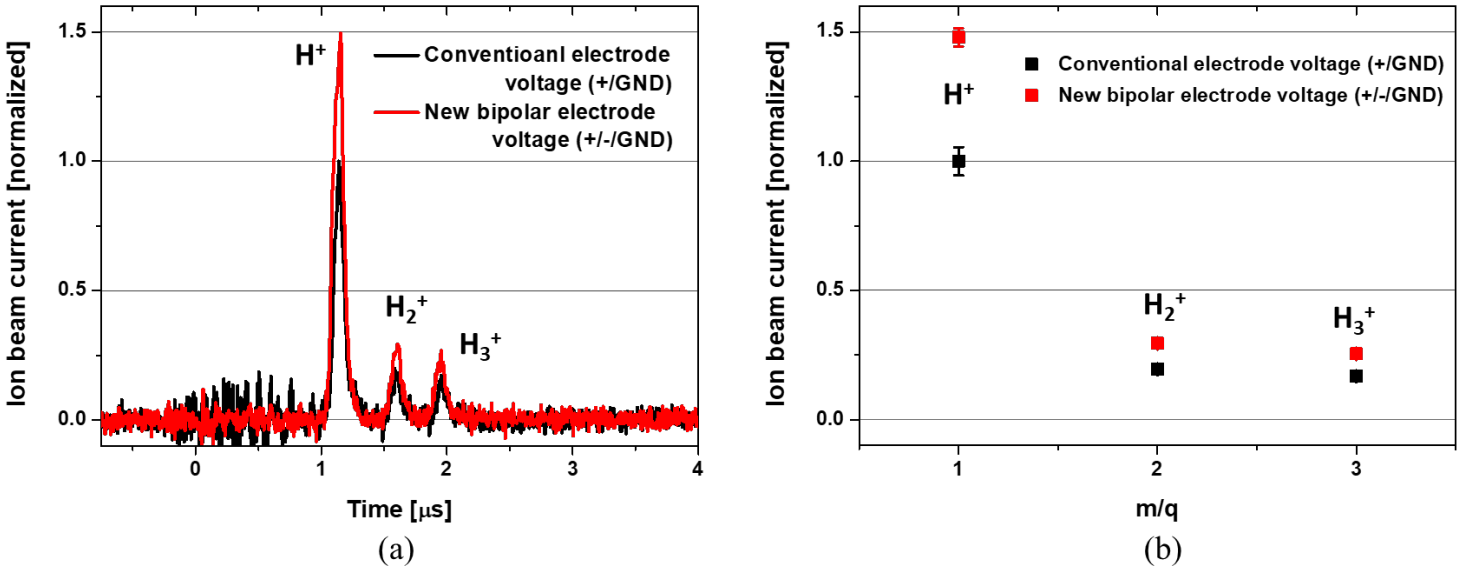

Figure 4.10 Comparison of the ion beam signal between the conventional method and newly developed one; (a) typical Faraday cup signals by a single measurement, (b) averaged peak values for fifty identical measurements.

The ion species fraction of hydrogen plasma produced by a Penning ion source is analyzed by the TOF system for various discharge currents from 2 A to 25 A at the operating pressure of 10 mTorr. Figure 4.11 shows that the monatomic fraction increases with increasing the discharge current. Since the discharge current is known to be proportional to the plasma density, the measured values are compared with the numerical results obtained from the in-house hydrogen numerical model [6,32,51]. for various plasma densities. The simulation results show good agreements with the ion species fraction measured by the TOF system with an improved gate device, indicating the good performance of the TOF system presented in this paper.

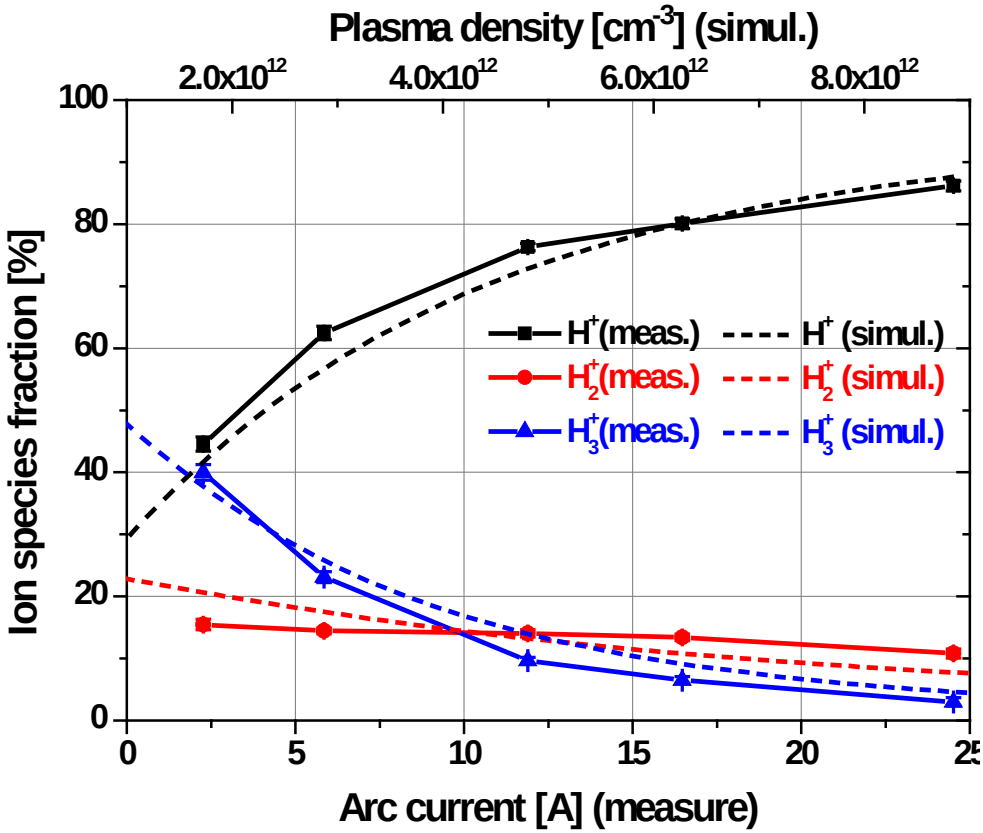

Figure 4.11 Variation of ion species fraction of hydrogen beam with discharge current for TOF measurement (solid curves) and comparison with the numerical calculation with plasma density (dashed curves)

Chapter 5 Experiments and Results

5.1 Experimental Setup and Operation Optimization

Hollow cold cathode Penning ion source was fabricated as shown in Figure 5.1. In the center, a tubular anode of 25 mm in inner diameter and 40 mm in length made of copper is placed. And a hollow cathode of 25 mm in inner diameter and 15 mm in length are placed on both sides of the anode. The hollow cathode was made of molybdenum to be resistant to erosion by sputtering. Between the anode and the cathodes, a 5 mm insulators in ceramic material make gaps. The axial magnetic field of the Penning ion source is applied by the solenoid electromagnet. The magnetic field of 100 G per 6 A solenoid current is applied in the center. Moving from 100 to 1500 G, the discharge characteristics are observed and the optimum operation point is searched. A 3 mm beam extraction hole was placed on one of two hollow cathodes and an extractor was installed with a 5 mm gap. For the time-of-flight mass analysis, the accelerating voltage V_{acc} is applied up to 10 kV. For the Penning plasma discharge, the discharge voltage V_{disch} is applied from 1 – 3 kV, and the discharge current was controlled by combining the discharge voltage and the limiting resistance R_{lim}. It was discharged with a pulse within 100 μs suitable for making an ion beam of 10 μs pulse width. The anode was grounded and negative voltage was applied to the cathodes for discharging. The original purpose of this study is a Penning ion source for the neutron generator. However, for the safety, hydrogen gas is discharged instead of deuterium so that unintentional neutron radiation would not occur.

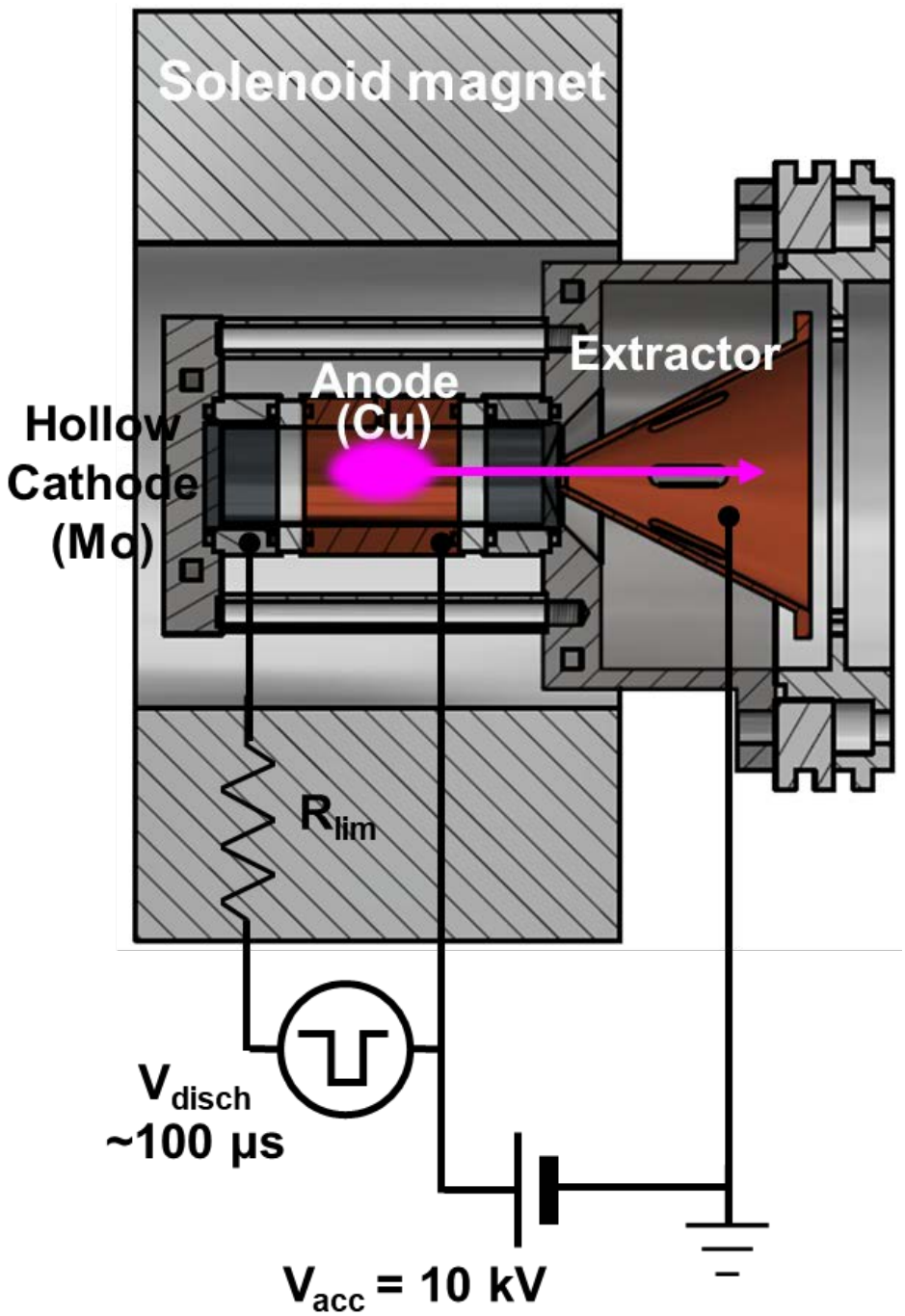

Figure 5.1 Hollow cold cathode Penning ion source in axial extraction.

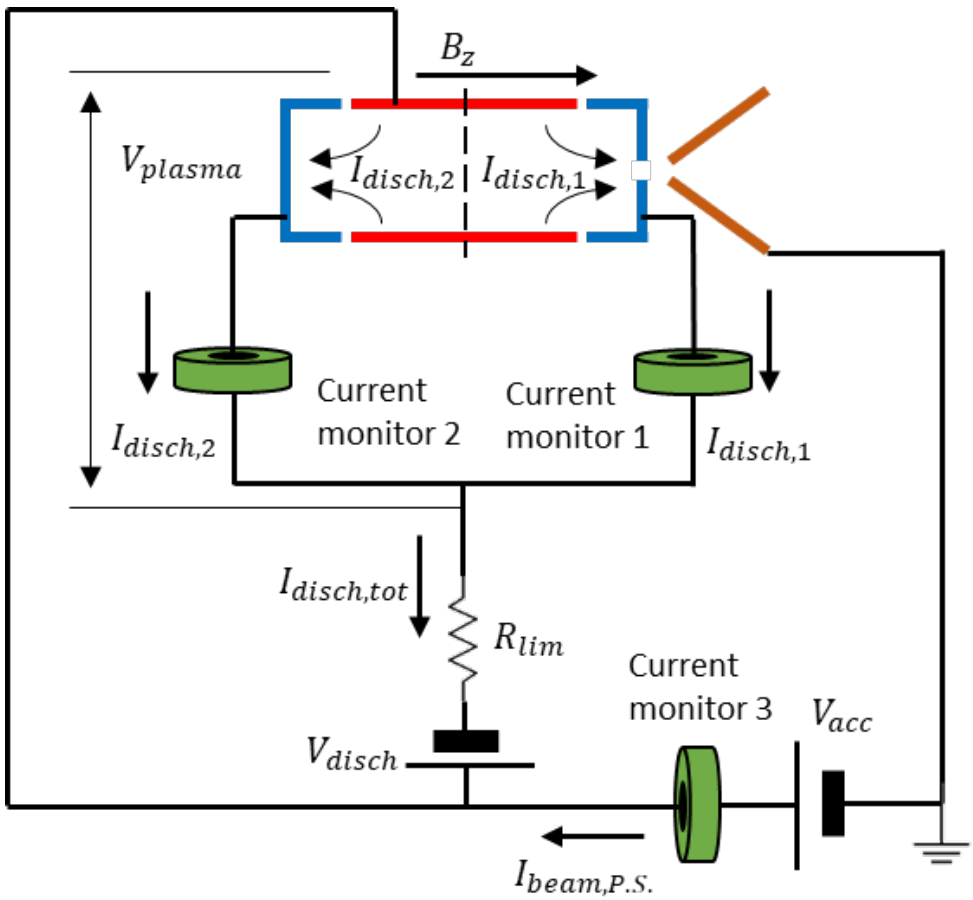

Figure 5.2 A schematic diagram of the current and the voltage relation in the ion source.

Figure 5.2 shows the relationship between the voltage and the current in the ion source. The discharge current in the Penning ion source is divided into two cathodes, and current monitors are installed to measure the current respectively. Another current monitor is installed to measure the current from the power supply for the accelerating voltage, which corresponds to extracted beam current. Figure 5.3 is typical waveforms of discharge current.

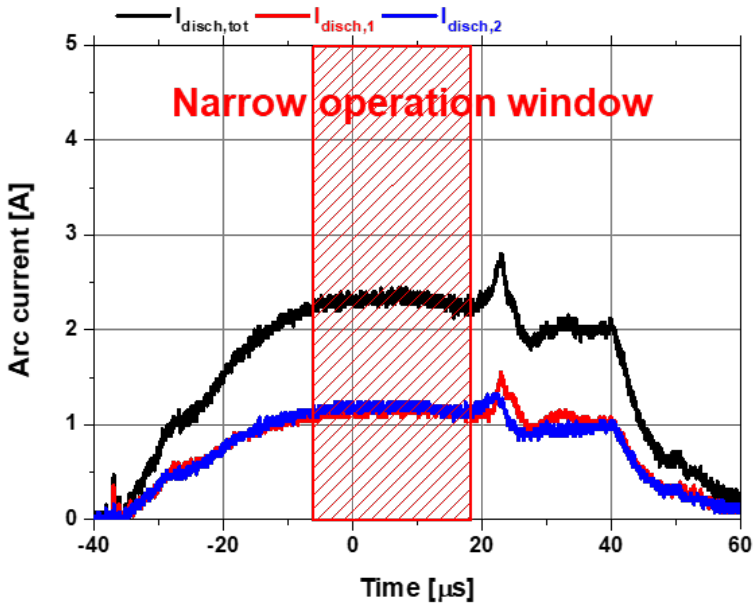

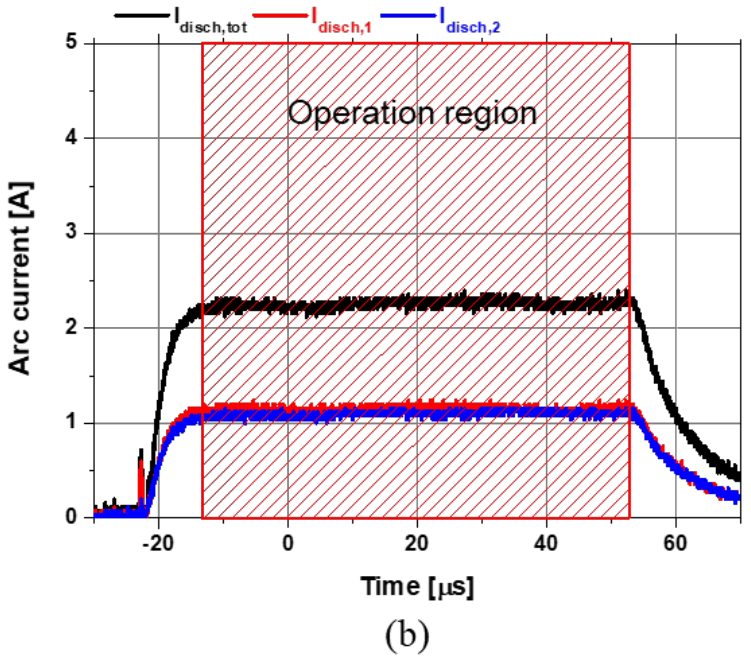

Figure 5.3 Typical waveform of discharge current; (a) hollow cathode Penning ion source, (b) general flat cathode Penning ion source.

Figure 5.3(a) is waveform for the hollow cathode Penning ion source, and Figure 5.3(b) is for the general flat cathode Penning ion source. The discharge is a stable mode in which the discharge current is uniformly distributed to both cathodes. While the discharge current is maintained long in the flat-top in the case of general flat cathodes, the time to form a flat-top is not long for the hollow cathodes. However, since the required time of 10 μs or more can be obtained, this discharge is used as it is.

The magnetic field is one of the important factors in the Penning ion source. Penning discharge is one of the crossed field discharges where the electric field and the magnetic field are perpendicular to each other. Therefore, E×B drift occurs in the plasma, which causes instability [52]. The larger the magnetic field, the larger the instability, but also the greater performance of confining the electrons, which also helps to improve the plasma density. Therefore, selecting the proper magnetic field is important for stable and good performance. Figure 5.4 is the result of the axial B-field scanning for searching the optimum operation point. Figure 5.4(a) is for the hollow cathode Penning ion source. In this case, the instability increases rapidly over 800 G. Under 800 G, ion species fraction does not change so much, but beam current has maximum around 700 G. So in the case of the hollow cathode, the experiment will be performed at the axial B-field 700 G. Figure 5.4(b) is for the general flat cathode. In this case, the instability increases over 800 G too, and the monatomic fraction and the beam current have maximum values at 350 G. So in the case of the general flat cathode, the experiment will be performed at 350 G.

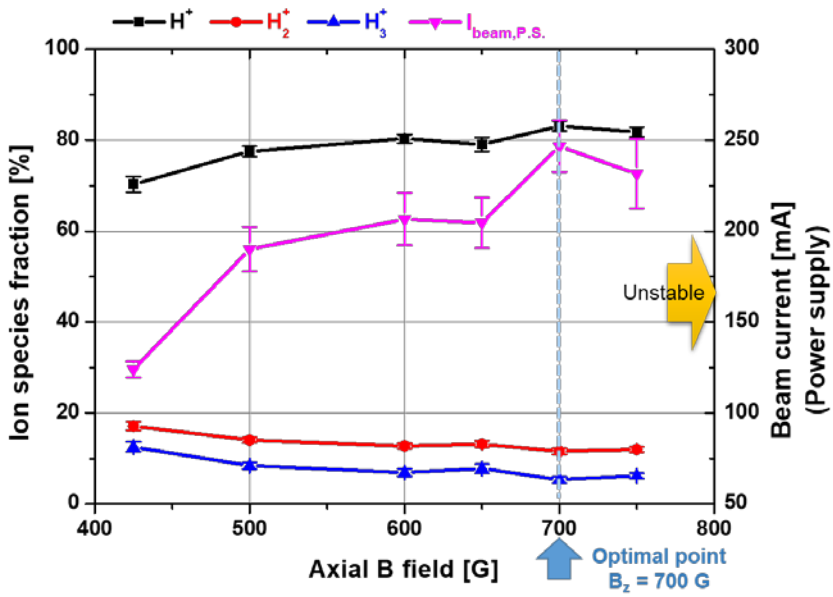

(a)

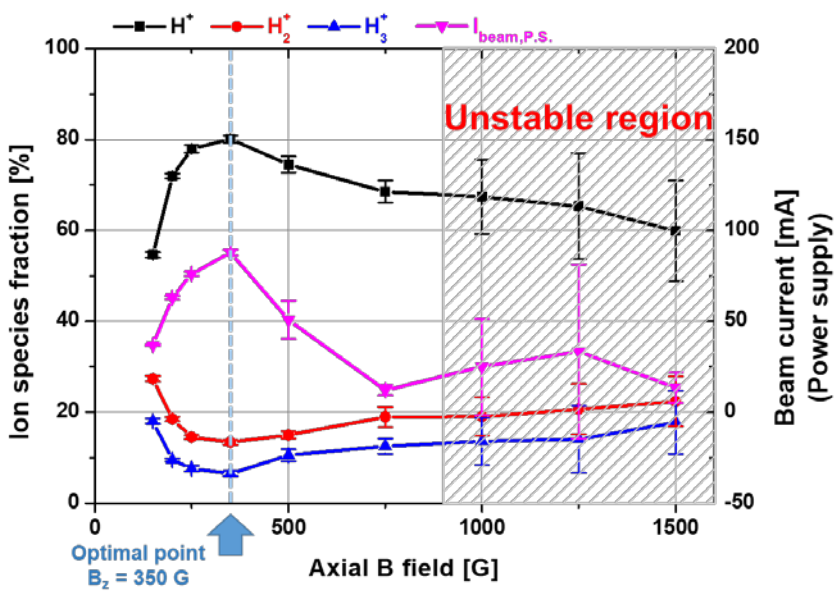

(b)

Figure 5.4 Axial B-field scanning for searching optimum operation; (a) hollow cathode Penning ion source, (b) general flat cathode Penning ion source.

This difference may come from that a hollow cathode discharge is responsible for a considerable part of the discharge, so instability is alleviated in a higher magnetic field. In this case, since the confinement performance of the higher magnetic field is increased, it also helps to improve the plasma density.

5.2 Ion Species Fraction of Penning Ion Source with Hollow Cathode

The ion species fraction was measured using the TOF mass analyzer prepared in the previous chapter with the experimental set up and operating conditions prepared in the previous section. In the case of the hollow cathode, the axial B-field is 700 G, and for the flat cathode, 350 G. Gas flow is 5 sccm. The change of ion species fraction is measured according to the discharge current. Figure 5.5 is the result.

The monatomic fraction of a commercial neutron generator device is under 10 %. However, the Penning ion source of this study with the hollow cathode shows the dramatic enhancement. The monatomic fraction of the hollow cathode Penning ion source is close to 60% at the same discharge current with a commercial device, about 2 A. 5 or 6 times enhancement is acquired. Considering cathode erosion, normal device has to be operated in low discharge current. But the hollow cathode discharge has advantage for cathode erosion, so higher discharge current operation is possible and higher monatomic fraction can be acquired. The monatomic fraction over 80% at the discharge current under 10 A is shown in Figure 5.5.

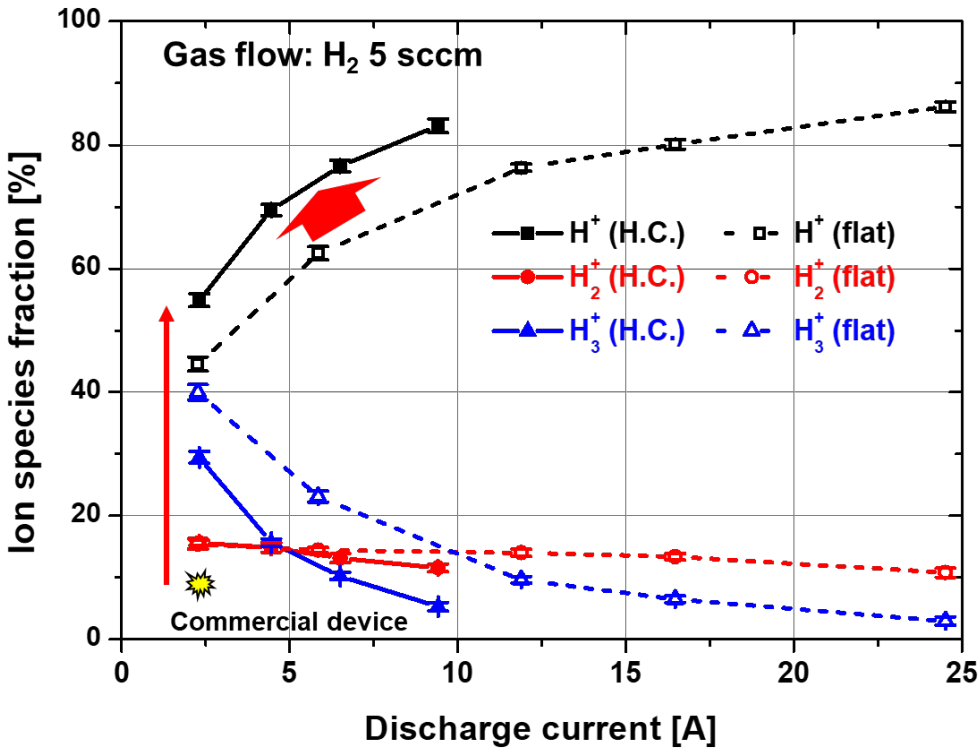

Figure 5.5 The result of measuring ion species fraction according to the discharge current. The hollow cathode Penning ion source (solid line) is operated in 350 G, and the flat cathode Penning ion source (dotted line) is operated in 700 G.

In case of the general flat cathode Penning ion source, the monatomic fraction is improved with the optimized operation. At the discharge current about 2 A, H^+ fraction is over 40%. Although a monatomic fraction can be improved by employing a hollow cathode structure, considerable improvements can be obtained by optimizing operating conditions in existing structures.

Figure 5.6 shows the change of ion species fraction by gas flow corresponding to the operating pressure. As discussed in Chapter 2, operating pressure also affects the monatomic fraction. At a low gas flow, monatomic fraction increases slightly. But at further low gas flow, the discharge is unstable. From this result, it can be seen that discharging at a low gas flow is advantageous for obtaining a higher monatomic fraction as long as the stability of the discharge is maintained.

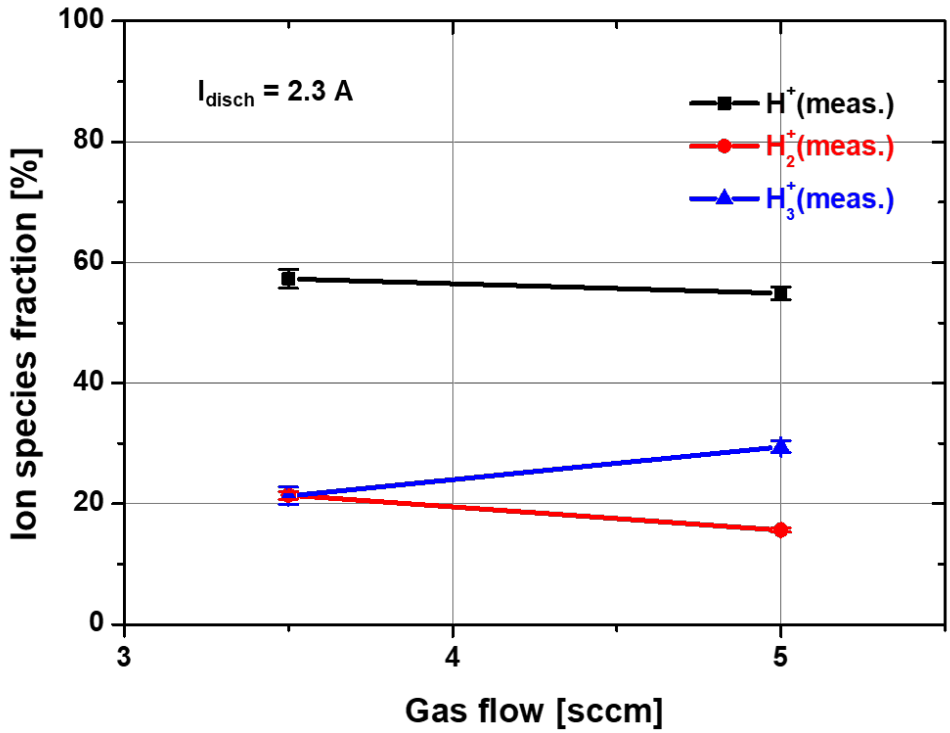

Figure 5.6 The change of ion species fraction by gas flow.

5.3 Ion Beam Current of Penning Ion Source with Hollow Cathode

The main focus of this study is on the monatomic fraction. However, the beam current also occupies an important position as a performance of the ion source. The ion beam current is proportional to the plasma density and proportional to the square root of the electron temperature. However, the monatomic fraction is advantageous as the electron temperature is lowered, so that the improvement of the monatomic fraction may have a bad influence on the beam current due to the lowering of the electron temperature. The most direct way to verify this is to measure plasma density and electron temperature. However, since the discharge is maintained in several tens of μs, and the recovery from the noise caused by the discharge initiation voltage is not sufficiently performed within the discharge period, it is impossible to measure the plasma parameters by the triple probe used for the pulse plasma discharge. Therefore, it is impossible to measure the changes in the plasma density and the electron temperature. However, it is desired to directly measure the beam current to confirm that there is no problem of the beam current decrease.

Figure 5.7 is an ion beam current measurement set up. Because of the limitations of the system, the beam optics are not good because the acceleration voltage can only be raised to 10 kV, so that most of the extracted beam goes to the extractor and the ion beam diverges although it passes through the extractor hole. So the current to the extractor should be measured and Faraday cup should be installed as close to the extractor as possible. In the Faraday cup, secondary electron emission is suppressed by magnetic field, but there is no suppression in the extractor. Therefore, the current to the extractor should be compensated.

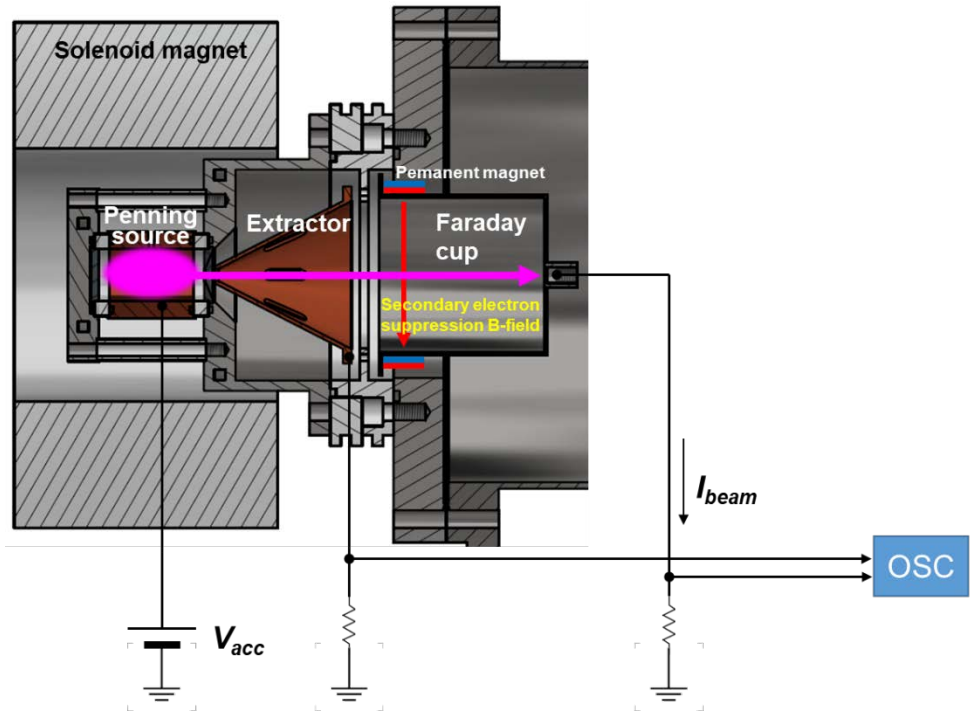

Figure 5.7 Ion beam current measurement set up.

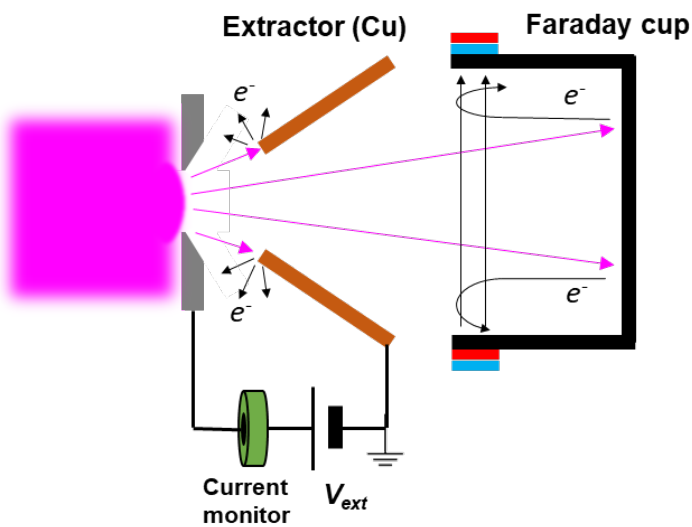

Figure 5.8 Schematic diagram of ion beam measurement

As shown in Figure 5.8, The electric field of the accelerating voltage is insufficient and the meniscus of the extraction hole is protruding and much of ion beam extracted goes to the extractor. To compensate the increase in beam current measured at the extractor, secondary electron emission coefficient of copper in bombardment of 10 keV hydrogen ion. From the literature, it is known as approximately 1 [53]. So the total ion beam current is decided that the current to the Faraday cup is added to the half of the current to the extractor.

In Figure 5.9, for the flat cathode, the current to the Faraday cup and the current to the extractor cross each other because beam optics goes well. But for the hollow cathode, this cross isn't shown because the plasma density of the hollow cathode case is higher than that of the flat cathode case. So I have to use the total current as the representative ion beam current.

Comparing the total currents in Figure 5.10, the ion beam current of the hollow cathode case is much higher than that of the flat cathode case. The beam current density was more than 2 times higher. From this result, it can be seen that this new Penning ion source performs well without damaging the beam current. At about 2 A discharge, over 200 mA beam current can be acquired through 0.2 cm^2 extraction hole.

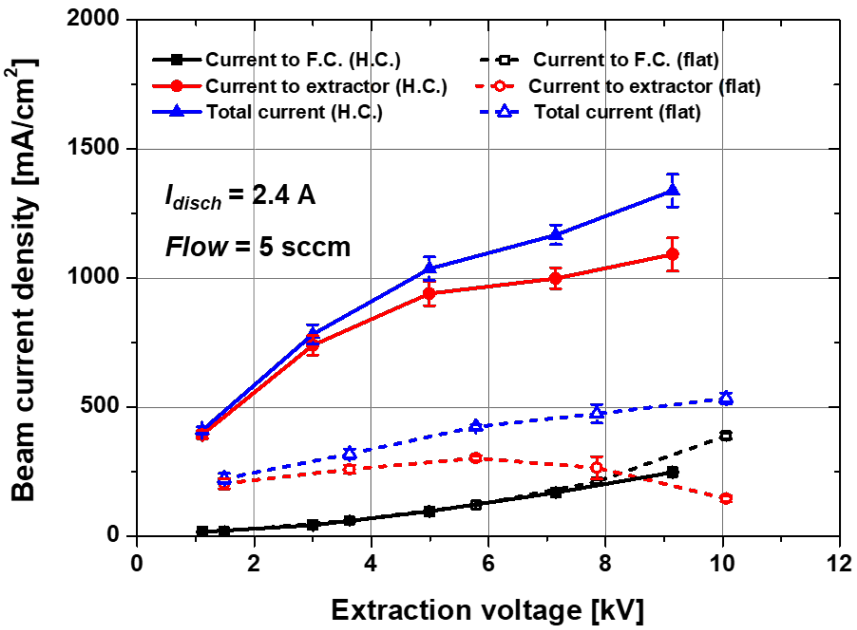

Figure 5.9 Measurement of ion beam current according to extraction (acceleration) voltage.

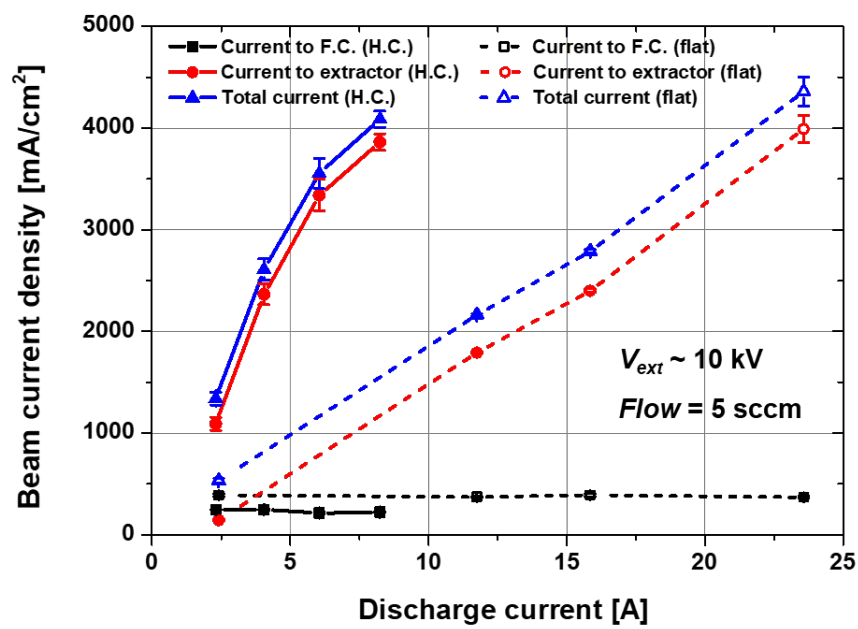

Figure 5.10 Measurement of ion beam current according to the discharge current.

Chapter 6 Summary and Conclusion

The hydrogen cold cathode Penning ion source with high monatomic fraction in pulsed operation is developed. As a hydrogen ion source, Penning ion source can have high plasma density and high monatomic fraction according to discharge condition. However, in neutron generator applications especially in sealed tube type, it has very low monatomic fraction due to the limitation in operation. In this study, it is aimed to develop a Penning ion source beyond this limitation.

Calculating the ion species fraction by using the reaction of hydrogen in the plasma and the particle balance equation, etc., it is found that the monatomic fraction increases at high plasma density, low electron temperature, and low operating pressure. Among them, the influence of the plasma density is most important. In order to increase efficiently, the plasma density in consideration of the system limitation, it is preferable to add the DC discharge concept using the same power system. A hollow cathode discharge is a good candidate. Hollow cathode discharge is capable of high density plasma discharge by itself due to the hollow cathode effect. Unlike a previous Penning ion source with a hollow cathode, in this study, hollow cathodes are installed to the beam extraction side and the opposite side symmetrically for discharge stability. When this structure is applied to the Penning ion source, more excellent performance is obtained. Apart from the fact that the hollow cathode can achieve a high plasma density, there is another advantage that it is strong against cathode erosion. This is also useful in this study.

A time-of-flight mass analyzer is developed to measure the ion species fraction of a short-time pulsed ion beam. the gating device, which is a core part, is modified to improve the signal-to-noise ratio over the existing device.

Ion species fraction is measured with a new Penning ion source with hollow cathodes. The monatomic fraction of commercial devices is reported to be about 10%. However, the monatomic fraction of our ion source increased by up to 60% at discharge current of about 2 A, which is a discharging condition same with commercial device. It is improvement of 5 – 6 times comparing to the commercial device. Moreover, when operating at a higher discharge current, it is possible to obtain a monatomic fraction of 70 – 80% or more. As for the beam current density, the new structure has more than twice the performance improvement compared to the existing structure.

In this study, the effect of plasma density enhancement by the hollow cathode effect is applied to the Penning ion source. Therefore, the limit of monatomic fraction of commercial devices is greatly resolved. This will be helpful to obtain higher performance in the field of applications of hydrogen Penning ion source, especially to obtain higher neutron yields in the field of the portable sealed tube neutron generators.

Bibliography

[1] H. Zhang (ed), Ion Sources, New York: Science Press, Springer, 1999.

[2] R. Scrivens, "Proton and Ion Sources for High Intensity Accelerators," in *Proceedings of EPAC 2004*, Lucerne, 2004.

[3] K. Choe, B. K. Jung, K.-J. Chung and Y. S. Hwang, "Development of a Radio Frequency Ion Source with Multi-Helicon Plasma Injectors for Neutral Beam Injection System of Versatile Experiment Spherical Torus," *Review of Scientific Instruments,* vol. 85, p. 02B318, 2014.

[4] B. K. Jung, K. -J. Chung, Y. H. An, J. Y. Park and Y. S. Hwang, "Development of a High-Current Ion Source with Slit Beam Extraction for Neutral Beam Injector of VEST," *Fusion Engineering and Design,* Vols. 96-97, p. 438, 2015.

[5] H. D. Jung, M. J. Park, S. H. Kim and Y. S. Hwang, "Development of a Compact Helicon Ion Source for Neutron Generators," *Review of Scientific Instruments,* vol. 75, pp. 1878-1880, 2004.

[6] H. D. Jung, J. Y. Park, K. J. Chung and Y. S. Hwang, "Development of a High-Current Helicon Ion Source with High Monoatomic Fraction for the Application of Neutron Generators," *IEEE Transactions on Plsama Science,* vol. 35, pp. 1476-1479, 2007.

[7] H.-J. Kwon, "Study on the Microwave Ion Source of the 100-MeV Proton Linac," *Journal of the Korean Physical Society,* vol. 69, pp. 967-970, 2016.

[8] H.-J. Kwon, "Study on the Beam Properties of the Microwave Ion Source,"

Journal of the Korean Physical Society, vol. 71, pp. 814-817, 2017.

[9] T.-S. Kim, S. H. Jeong, D. H. Chang, K. W. Lee and S.-R. In, "Performance of a New Ion Source for KSTAR Tokamak Plasma Heating," *Plasma Science and Technology,* vol. 16, pp. 620-624, 2014.

[10] R. S. Hemsworth and T. Inoue, "Positive and Negative Ion Sources for Magnetic Fusion," *IEEE Transations on Plasma Science,* vol. 33, pp. 1799-1813, 2005.

[11] N. Akino, N. Ebisawa, A. Honda, Y. Ikeda, M. Kawai, M. Kazawa, K. Mogaki, T. Ohga, N. Umeda, K. Usui, T. Yamamoto and L. Grisham, "Long Pulse Operation on NBI Systems for JT-60U," *Fusion Science and Technology,* vol. 47, pp. 758-762, 2005.

[12] O. Waldmann and B. Ludewigt, "Measurements of beam current density and proton fraction of a permanent-magnet microwave ion source," *Review of Scientific Instruments,* vol. 82, p. 113505, 2011.

[13] A. Sy, Q. Ji, A. Persaud, O. Waldmann and T. Schenkel, "Novel methods for improvement of a Penning ion source for neutron generator applications," *Review of Scientific Instruments,* vol. 83, p. 02B309, 2012.

[14] L. A. Shope, R. S. Berg, M. L. O'Neal and B. E. Barnaby, "The Operation and Life of the Zetatron Neutron Tube in a Borehole Logging Application," *The International Journal of Applied Radiation and Isotopes,* vol. 34, pp. 269-272, 1983.

[15] E. J. T. Burns and G. C. Bischoff, "Ion Sources for Sealed Neutron Tubes, SAND97-2784C," Sandia National Laboratories, Albuquerque, NM, 1996.

[16] IAEA, IAEA Radiation Technology Reports Series No. 1: Neutron Generators for Analytical Purpose, Vienna: International Atomic Energy Agency, 2012.

[17] V. Valkovic, 14 MeV Neutrons: Physics and Applications, Boca Raton, FL: CRC Press, 2016.

[18] Y. S. Hwang, et al., "Development Project of Design and Fabricating Technology on High Performance and Small Size Pulse Mode Ion Beam Accelerating System," Agency for Defense Development, ADD-420, 2016.

[19] "Tables of Physical & Chemical Constants," National Physical Laboratory, 2017. [Online]. Available: http://www.kayelaby.npl.co.uk/atomic_and_nuclear_physics/4_7/4_7_4a.html.

[20] B. Wolf (ed), Handbook of Ion Sources, Boca Raton, FL: CRC Press, 1995.

[21] J. R. J. Bennet, "A Review of PIG Sources for Multiply Charged Heavy Ions," *IEEE Transactions on Nuclear Science,* vol. 19, pp. 48-68, 1972.

[22] I. G. Brown (ed), The Physics and Technology of Ion Sources, New York: Wiley, 1989.

[23] W. Schuurman, "Investigation of a Low Pressure Penning Discharge," *Physica,* vol. 36, pp. 136-160, 1967.

[24] S. N. Abolmasov, "Physics and engineering of crossed-field discharge devices," *Plasma Sources Science and Technology,* vol. 21, p. 035006, 2012.

[25] O. Fukumasa, R. Itatani and S. Saeki, "Numerical simulation of hydrogen

ion species in the steady-state plasma of a low-pressure ion source," *Journal of Physics D: Applied Physics,* vol. 18, pp. 2433-2449, 1985.

[26] H. D. Jung, Compact hydrogen helicon plasma ion source with high current density and high monoatomic beam ratio, Ph. D. dissertation, Seoul National University, 2009.

[27] R. Zorat and D. Vender, "Global model for an rf hydrogen inductive plasma discharge in the deuterium negative ion source experiment including negative ions," *Journal of Physics D: Applied Physics,* vol. 33, pp. 1728-1735, 2000.

[28] K. -J. Chung, J. -J. Dang, J. Y. Kim, W. H. Cho and Y. S. Hwang, "Kinetics of Electrons and Neutral Particles in Radio-frequency Transformer Coupled Plasma H- Ion Source at Seoul National University," *New Journal of Physics,* vol. 18, p. 105006, 2016.

[29] R. K. Janev, W. D. Langer, K. Evans, Jr. and D. E. Post, Jr., Elementary Processes in Hydrogen–Helium Plasmas, Berlin: Springer-Verlag, 1987.

[30] R. Zorat, J. Goss, D. Boilson and D. Vender, "Global model of a radiofrequency H2 plasma in DENISE," *Plasma Sources Science and Technology,* vol. 9, pp. 161-168, 2000.

[31] M. A. Lieberman and A. J. Lichtenberg, Principles of Plasma Discharges and Materials Processing, Hoboken, NJ: John Wiley & Sons, 2005.

[32] K.-J. Chung, B.-K. Jung, Y. An, J.-J. Dang and Y. S. Hwang, "Effects of discharge chamber length on the negative ion generation in volume-produced negative hydrogen ion source," *Review of Scientific Instruments,* vol. 85, p. 02B119, 2014.

[33] I. G. Brown, J. E. Galvin, B. F. Gavin and R. A. MacGill, "Effect of resonant microwave power on a Penning ionization gauge ion source," *Review of Scientific Instruments,* vol. 56, pp. 1894-1896, 1985.

[34] Y. Yoshida, T. Ohnishi, Y. Hirofuji and T. Ikeda, "Sputtering ion source with simultaneous use of microwave and Penning-ionization-gauge discharge," *Review of Scieitific Instruments,* vol. 61, pp. 598-600, 1990.

[35] S. N. Abolmasov, M. Shindo, M. V. Buttlar, H. Muta, A. A. Bizyukov and Y. Kawai, "Development of a hybrid PIG-ECR ion source," *Surface and Coatings Technology,* vol. 174 –175, p. 142–146, 2003.

[36] M. Ma, J. E. Mynard, B. J. Sealy and K. G. Stephens, "A cold-hollow-cathode lateral-extraction Penning ion source," *Nuclear Instruments and Methods in Physics Research B,* vol. 55, pp. 335-338, 1991.

[37] I. Osipov and N. Rempe, "A plasma–cathode electron source designed for industrial use," *Review of Scientific Instruments,* vol. 71, pp. 1638-1641, 2000.

[38] E. Oks, M. Shandrikov, C. Salvadori and I. Brown, "Low-energy dc ion source for low operating pressure," *Review of Scientific Instruments,* vol. 85, p. 083502, 2014.

[39] V. I. Kolobov and L. D. Tsendin, "Analytic model of the hollow cathode effect," *Plasma Sources Science and Technology,* vol. 4, pp. 551-160, 1995.

[40] R. V. Kennedy, "Theory of the arc hollow cathode," *Journal of Physics D: Applied Physics,* vol. 34, p. 787–793, 2001.

[41] H. Eichhorn, K. H. Schoenbach and T. Tessnow, "Paschen's law for a hollow cathode discharge," *Applied Physics Letter,* vol. 63, pp. 2481-2483,

1993.

[42] V. I. Kolobov and A. S. Metel, "Glow discharges with electrostatic confinement of fast electrons," *Journal of Physics D: Applied Physics*, vol. 42, p. 233001, 2015.

[43] E. M. Oks, M. V. Shandrikov and A. V. Vizir, "Operating modes of a hydrogen ion source based on a hollow-cathode pulsed Penning discharge," *Review of Scientific Instuments*, vol. 87, p. 02B703, 2016.

[44] E. de Hoffmann and V. Stroobant, Mass Spectrometry: Principles and Applications, 3rd Ed., West Sussex, England: John Wiley & Sons, 2007.

[45] F. Hillenkamp, M. Karas, R. C. Beavis and B. T. Chait, "Matrix-Assisted Laser Desorption/Ionization Mass Spectrometry of Biopolymers," *Analytical Chemistry*, vol. 63, pp. 1193A-1203A, 1991.

[46] M. Guilhaus, V. Mlynski and D. Selby, "Perfect Timing: Time-of-flight Mass Spectrometry," *Rapid Communications in Mass Spectrometry*, vol. 11, pp. 951-962, 1997.

[47] I. G. Brown, J. E. Galvin, R. A. MacGill and R. T. Wright, "Improved time-of-flight ion charge state diagnostic," *Review of Scientific Instruments*, vol. 58, pp. 1589-1592, 1987.

[48] I. G. Brown, B. Feinberg and E. J. Galvin, "Multiply stripped ion generation in the metal vapor vacuum arc," *Journal of Applied Physics*, vol. 63, pp. 4889-4898, 1988.

[49] V. I. Gushenets, A. G. Nikolaev, E. M. Oks, L. G. Vintizenko, G. Y. Yushkov, A. Oztarhan and I. G. Brown, "Simple and inexpensive time-of-flight charge-to-mass analyzer for ion beam source characterization,"

Review of Scientific Instruments, vol. 77, p. 063301, 2006.

[50] V. I. Gushenets, A. S. Bugaev, E. M. Oks, G. Y. Yushkov, A. Hershcovitch, B. M. Johnson, T. V. Kulevoy, H. J. Poole and A. Y. Swarovsky, "Generation of a boron ion beam in a modified ion source for semiconductor applications," *Review of Scientific Instruments,* vol. 77, p. 03C109, 2006.

[51] K. Choe, K.-J. Chung and Y. S. Hwang, "Modeling and Measurement of Hydrogen Ion Species Fractions in a Penning Plasma Discharge," in *Transactions of the Korean Nuclear Society Spring Meeting, 17S-973*, Jeju, Korea, 2017.

[52] F. C. Hoh, "Instability of Penning-Type Discharges," *The Physics of Fluids,* vol. 6, pp. 1184-1191, 1963.

[53] J. W. Murdock and G. H. Miller, "Secondary electron emission due to positive ion bombardment," Ames Laboratory ISC Technical Reports 106, 1955.

국문 초록

수소(양성자 또는 중수소) 이온원은 양성자 가속기의 입사기, 핵융합의 중성입자빔 입사장치, 중성자 발생장치 등에서 핵심적인 부분을 차지한다. 이온원의 가장 대표적인 성능 요소는 이온 빔 전류로, 빔 전류가 클수록 목표하는 반응의 수율을 높일 수 있다. 수소 이온원의 경우 그와 함께 단원자 분율도 중요한 성능 요소가 된다. 수소 이온 빔은 단원자 이온(양성자, H^+ 또는 중양자, D^+) 뿐만 아니라 분자 이온(H_2^+(D_2^+), H_3^+(D_3^+))도 포함하고 있다. 이온 빔 내 단원자 이온은 분자 이온에 비해 핵자 당 가지는 에너지가 커서, 이온 빔이 목표로 하는 반응의 수율을 향상 시킬 수 이다. 그리하여 단원자 분율이 높을수록 이온원의 성능에 유리하다. 수소 이온원의 응용 분야 중, 휴대형 밀봉 튜브 중성자 발생장치에는 구조가 단순하고 전원 구성이 쉬운 페닝 이온원이 주로 사용된다. 페닝 플라즈마 방전은 양극과 음극의 구조 및 자기장으로 전자를 더 많이 구속하여, 낮은 압력에서도 높은 밀도의 플라즈마를 발생시키는 장점이 있다. 그러나 휴대형 밀봉 튜브의 경우, 이 방식이 가지는 제한으로 단원자 분율은 10% 정도 밖에 되지 않는다. 따라서 단원자 분율을 개선하면 그 이온 빔을 이용하는 장치의 성능 또한 향상시킬 수 있다. 본 연구에서는 단원자 분율의 한계를 개선하여 해당 이온원의 성능을 높이고자 한다.

수소 플라즈마 내에서 일어나는 전자와 수소 분자, 원자, 이온의 충돌 반응을 기반으로, 각 이온 종(種)과 원자 분자의 생성과 소멸을 반영한 입자균형방정식 등의 수식을 연립하여 계산하면, 플라즈마 조건에 따른 이온종 분율을 예측할 수 있다. 이러한 계산 모델을 통해, 플라즈마 밀도가 높을수록, 전자 온도가 낮을수록, 그리고 운전 압력이

낮을 수록 수소 이온 빔의 단원자 분율이 높아짐을 알 수 있다. 이런 플라즈마의 조건들을 조정하면 이온 빔의 단원자 분율을 향상시킬 수 있다.

단원자 분율에 영향을 주는 플라즈마의 조건 중 플라즈마 밀도가 가장 큰 역할을 한다. 플라즈마 밀도는 방전 시 전력을 많이 인가하면 쉽게 상승하지만, 비용이 많이 들고 기기의 손상을 가속화 시킨다. 특히 휴대형 기기의 경우, 구조와 전원 장치에 제약이 있어, 전력을 무한히 공급할 수 없다. 그리하여 페닝 이온원의 직류 방전 전원 시스템을 함께 이용할 수 있고, 구조 변경에도 간단한 공동 음극(hollow cathode) 구조를 페닝 이온원에 적용하였다. 공동 음극 효과(hollow cathode effect)로 인한 플라즈마 밀도 향상이 페닝 방전과 결합하면서 높은 단원자 분율을 얻을 수 있다. 이 외에, 공동 음극이 가진 음극 손상에 대한 내성으로 기기의 수명을 늘일 수 있는 장점도 있다.

수소 이온 빔의 이온 종 분율 측정을 위해서는 비행시간 측정 질량 분석기(time-of-flight mass analyzer)를 제작하여 측정하였다. 이온 빔의 질량 대 전하 비(mass-to-charge ratio)를 측정하는 데는 일반적으로 자기장을 이용하지만, 짧은 펄스로 생성되는 플라즈마의 이온 종 분율을 측정하는 데는 자기장의 변화 속도가 늦어서 적절하지 않다. 그래서 짧은 빔 펄스 패킷만으로도 이온 종 분율 측정이 가능한 비행시간 측정 질량 분석기를 개발하였다. 특히 이 연구에서는 이온 빔을 짧은 펄스 패킷으로 잘라내는 데 핵심 부품인 게이팅 장치(gating device) 를 개선하여 측정 신호의 신호 대 잡음 비(signal-to-noise ratio)를 50% 가량 향상시켰다.

공동 음극 적용 페닝 이온원의 운전을 최적화 시켜 축 방향 자기장 700 G 에서 운전하였다. 음극의 손상 방지를 고려하여 약 2 A 방전

전류로 운전했을 때, 기존의 기기의 성능인 약 10% 단원자 분율에 비해, 5 – 6 배 향상된 성능인 60%에 가까운 단원자 분율을 얻을 수 있었다. 빔 전류에 있어서도 함께 실험한 일반 평면 음극 페닝 이온원에 비해 2 배 이상의 빔 전류 밀도를 보였다.

이 연구의 성과를 적용하면 향후 페닝 이온원 응용 분야의 발전에 도움을 줄 수 있을 것이며, 특히 휴대형 밀봉 튜브 중성자 발생장치 분야에서 향상된 성능을 보여 줄 것으로 기대된다.

주요어: 페닝 이온원, 수소 이온 빔, 중성자 발생 장치, 단원자 분율, 공동 음극, 비행시간 질량 분석

학 번: 2013-30300